

POLITECNICO DI TORINO



Master's Thesis in Mechatronic Engineering

Control of fast pick and place Direct Drive DELTA robot

Effects of different control strategies and robot segments

Internal supervisor
Prof. Andrea Tonoli

Federico ALLIONE
Student ID: 240286

External supervisor at
École Polytechnique Fédérale de Lausanne
Dr. Mohamed Bouri

ACADEMIC YEAR 2017 – 2018

Summary

The aim of this project was to implement and compare different control strategies on a Delta Direct Drive parallel robot available at the Laboratory of Robotic Systems (head of department Professor Hannes Bleuler, team leader Doctor Mohamed Bouri; supervisor at Politecnico di Torino Professor Andrea Tonoli), École Polytechnique Fédérale de Lausanne Switzerland (EPFL), March-July 2018. The performances of arm segments with different rigidity have been analysed. The controllers evaluated were the PID, the robust integral of signum of error (RISE) controller and an iterative learning controller based on the PID.

The robot studied in this project was the Direct Drive Delta robot with three degrees of freedom (3-DoFs). The purpose of this robot is to perform high speed pick and place operations. The actuation was without gearbox in order to increase the dynamic of the movements performed by the manipulator. The drawback of this choice is that all disturbances affecting the robot as well as changes of inertia have effect directly on the motors, without being mitigated by a gearbox. Due to this situation, the controller has to be as precise as possible in order to compensate for disturbances. A broad set of components of the robot were available and were tested in order to identify the best possible configuration. In the attempt of carrying out a proper comparison, all combinations of the components were tested using the same end effector, working conditions and trajectory. The state of the art I started from consisted on the one hand in robot links generally made of aluminium and on the other hand in control systems used only in simulation or in particularly favourable conditions.

My purpose was to test a set of hypotheses in order to find out the best combination between robot configuration and controller, with the intent of (1) optimising the working of the manipulator, (2) integrating new components into the dynamic model of the manipulator and (3) clarifying strengths and weaknesses of each controller implemented.

The present work is divided into two parts. The first one contains an introductory chapter and describes the test bench, both hardware and software aspects. The dynamic model of the robot used in this project, as taken from the literature, is also briefly exposed, since it has been widely mentioned in the continuation of the work.

The second part illustrates the controllers adopted and the performances obtained. For each controller a brief description of the method of operation is presented, followed by the measures obtained. We took care of testing the controllers under the same working conditions in order to reach comparable results. Moreover, the resonance frequency was investigated with the intent of reducing its effects. Digital filters have been designed and applied to remove this specific frequency. The performances, of the two performed experiments, have been evaluated by means of the root mean square error (RMSE) and

the peak errors of the Cartesian variables.

Experiment 1 - It consisted in assessing which is the best combination of arm segments and various control systems. The sampling frequency was set at 2 kHz and digital filters were applied. The controllers tested were the PID, the RISE and the Adaptive RISE. Obtained results clearly showed an improvement in the performances when the material of the links is carbon fibre instead of aluminium regardless the used controller.

Experiment 2 - It mainly focused in evaluating the best controller for fast pick and place operations of an unknown mass, while applying different levels of acceleration of the end effector in the workspace. The sampling frequency was reduced to 1 kHz and no digital filter was applied. None of the three previously mentioned controllers proved to be able to guarantee significantly better performances with respect to the others. Due to these results, I decided to implement an Iterative Learning Controller (ILC) based on a PID structure. On account of the extremely long time (more than half an hour) required by the ILC controller to auto-tune itself, this option was discarded as well.

The whole process required very high degrees of precision and accuracy, both as regards the definition of the different configurations and the monitoring effort. The thoroughly systematic observations of performances of controllers revealed that none of them was successful at the level I was looking for and consequently there is still room for improvement in this field by trying different solutions.

Material-wise my observations clearly showed that the carbon fibre solution outclassed the aluminium one.

My final results suggested therefore that a combination of carbon fibre links and an improved control system can still substantially enhance the performances of the direct drive delta robot.

During my testing exercises, I also happened to observe that the resonance frequency of the robot was varying according to the position of the mobile platform in the workspace. Therefore I suggest that it might be useful to investigate the relationship between physical position and frequency of resonance with the aim of obtaining an adaptive notch filter, in which the frequency cut should be a function of the position of the end effector in the space. Thus the dynamic of the system would not be limited by a wide band-stop filter, probably allowing better performances.

Contents

1	The DELTA robot	7
1.1	The direct drive Delta robot	9
1.2	The control system	13
1.3	Dynamic model	14
2	PID controller and resonance frequency	19
2.1	The PID controller	19
2.2	Effect of the feedforward torque	20
2.3	Resonance frequency	22
2.4	Performance comparison between arms	25
3	RISE and Adaptive RISE controllers	31
3.1	Structure of the RISE controller	31
3.2	Estimation of the transported mass	32
3.3	Estimation of the inertia of the arm	39
4	Comparison of different controllers in pick and place operations	43
4.1	Situation 1 - no mass transported	45
4.2	Situation 2 - 225 g mass attached to the mobile platform	47
4.3	Situation 3 - pick and place of a mass of 225 g	49
5	Iterative learning controller	55
5.1	Situation 1 - no mass transported	56
5.2	Situation 2 - 225 g mass attached to the mobile platform	58
5.3	Situation 3 - pick and place of a mass of 225 g	59
6	Conclusion	61
	Bibliography	63

Chapter 1

The DELTA robot

It is imperative to incorporate developments in digital technology and science of materials in existing machines in order to enhance the performances at the highest possible level. In particular control systems techniques and differential performance of component materials seem to be extremely relevant and are the main object of this research project.

The Delta robot is a parallel kinematic manipulator. It has been patented by Raymond Clavel [7] at the École Polytechnique Fédérale de Lausanne (EPFL) in the early eighties with the intent of packing chocolate pralines. It consists of three actuated kinematic chains linked together at the end to a mobile platform. Each chain is structured as follows:

- a revolutive actuator
- an arm connected to the actuator
- a forearm, made with two parallel rods forming a parallelogram, connected to the arm through ball-and-socket passive joints
- a mobile platform which links the three chains together by means of ball-and-socket passive joints.

Thanks to the physical structure of the manipulator, the mobile platform is always parallel to the base and it has only three degrees of freedom (DoF) along the Cartesian axes x , y and z . The orientation of the mobile platform is fixed (Figure 1.1). Other versions of the Delta robot allow also a rotation of the end effector around the z -axis (Figure 1.2).

The main characteristic of a parallel kinematic manipulator is that the base and the end effector are connected by more than one kinematic chain. In case of Delta robot the chains are three, the actuators are placed on the fixed base allowing the kinematic chains to be extremely light but at the same time the whole structure is very rigid. The movement of the mobile platform in the space (x,y,z) is given by the combination of movements of all the three actuators. The characteristic structure of the Delta robot allows the mobile platform to maintain the same orientation in the space regardless the position of the actuators and to remain parallel to the plane where the rotation axes of the motors lay. In order to make possible a fast displacement, arms, forearms and mobile platform have been built using light and stiff material such as aluminium and carbon fibre. Since the motors are placed on the fixed base, their weight and dimension do not influence the performances of

the robot. Because of that, direct drive motors (usually discarded in serial manipulators because big and heavy) are commonly used in Delta robots, since they allow more reactive and precise movements. Moreover the removal of the gearbox allows an easier design and assembling of the robot itself. However the absence of the gearbox require a more precise controller, able to compensate all the disturbances that affect the manipulator. In fact the mitigating action of the gearbox is not present, due to the absence of the gearbox itself.

Figure 1.1. Delta robot 3DoF

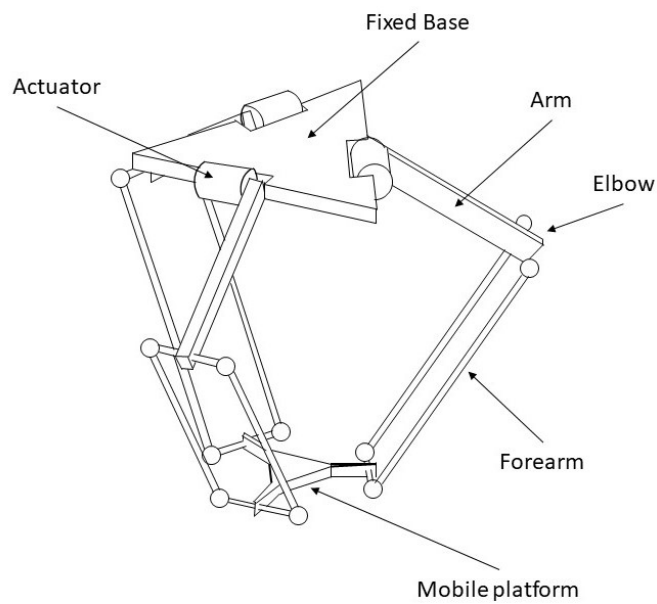
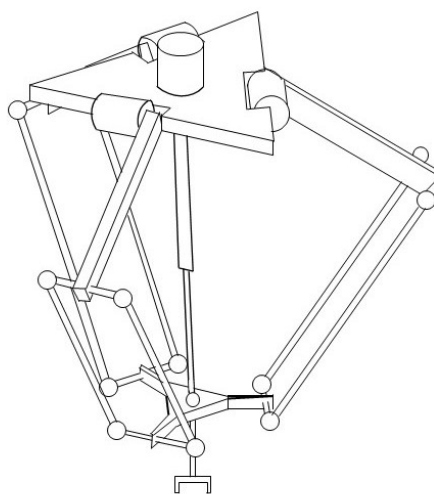


Figure 1.2. Delta robot 4DoF



1.1 The direct drive Delta robot

The robot used in this project is the direct drive Delta robot present at the laboratory of system robotics (LSRO) of the EPFL (Figure 1.3). Designed, assembled and controlled by Dr Mohamed Bouri.

Figure 1.3. Direct drive Delta robot used in the project



It is composed of three direct drive motors, each of them mounted on the fixed base and able to deliver up to 20 Nm of maximum torque, the inertia of the motor is $1.82 \cdot 10^{-3} \text{ Kg m}^2$. Each motor is directly connected to a single arm. Two types of arms are available, the first one made of aluminium (Figure 1.4) and the second one made of carbon fibre (Figure 1.5). Each arm is connected to the mobile platform with two parallel bars linked to both arm and mobile platform by means of ball-and-socket passive joints. The two bars are connected together with two springs allowing them to remain parallel to each other while the robot is moving. The whole structure is called forearm. Three types of forearms are available, each one made of carbon fibre but with different weight and joints. The first one (Figure 1.6) is characterized by a white coloured peek coupling case with a spherical socket (from now on referred as WPS). The second one (Figure 1.7) has a blue coloured aluminium coupling case with conical socket (referred as BAC). The last one (Figure 1.8) is a mixture of the previous two, in fact it has a grey coloured aluminium coupling case with spherical socket (referred as GAS). The three kind of forearms have been designed in order to evaluate the effects of the slightly different coupling systems and how the material of the case and the shape of the socket could affect the performances. The figures 2.11, 2.12 and 2.13 show more in detail the sockets of the forearms. The characteristic geometrical and dynamical quantities of all the arms and forearms are shown in the table 1.1. The spherical socket creates a wider contact surface with respect to the conical one. Because of that the friction is higher and it is more difficult to be compensated by the controller.

The end effector, called mobile platform (Figure 1.12), is made of aluminium and has a magnet attached under it, allowing transportation of light ferromagnetic objects. The mass of the mobile platform with the magnet is $m_p = 160 \text{ g}$.

Table 1.1. Geometric and dynamic parameters

	Length [cm]	Weight [g]
WPS	48	70
BAC	48	80
GAS	48	95
Aluminum arm	24	65
Carbon fibre arm	24	70

Figure 1.4. Aluminium arm



Figure 1.5. Carbon fibre arm



Figure 1.6. Forearm with peek coupling and spherical socket (WPS)



Figure 1.7. Forearm with aluminium coupling and conical socket (BAC)



Figure 1.8. Forearm with aluminium coupling and spherical socket (GAS)



Figure 1.9. Forearm with peek coupling and spherical socket (WPS)



Figure 1.10. Forearm with aluminium coupling and conical socket (BAC)

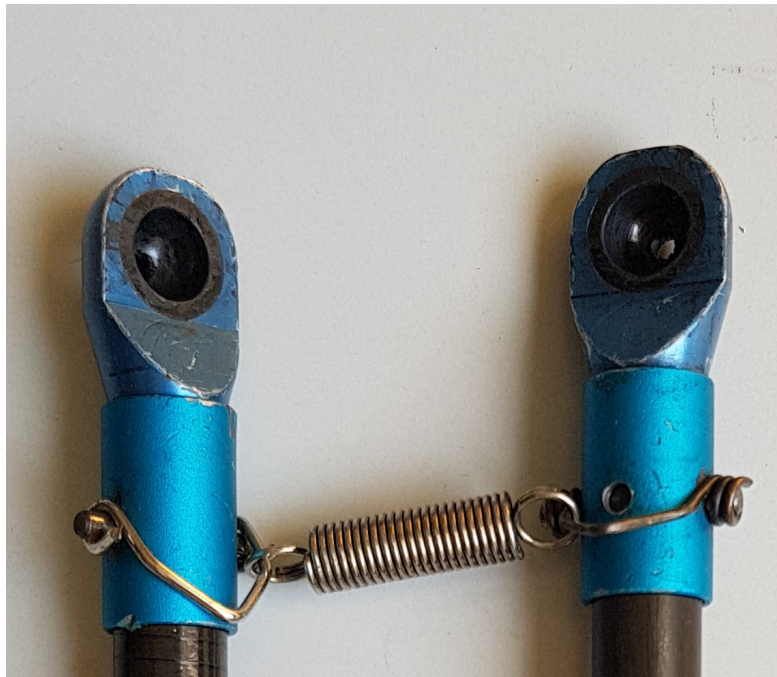


Figure 1.11. Forearm with aluminium coupling and spherical socket (GAS)

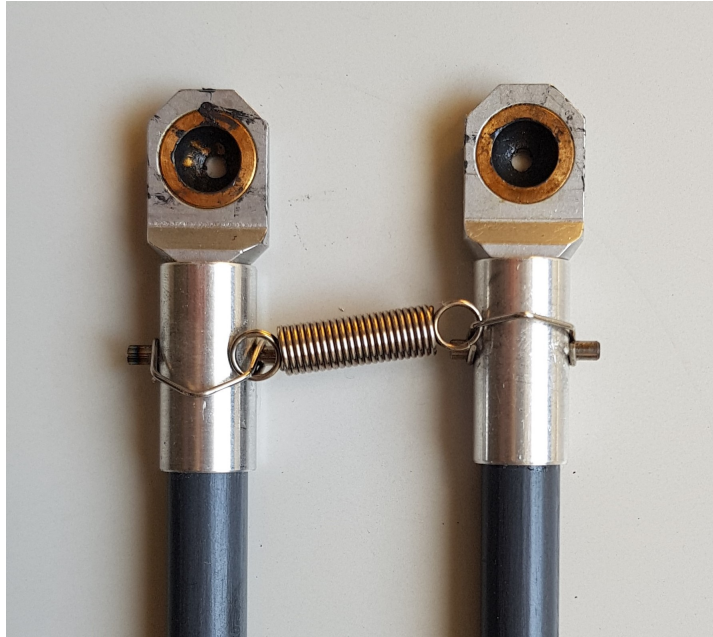
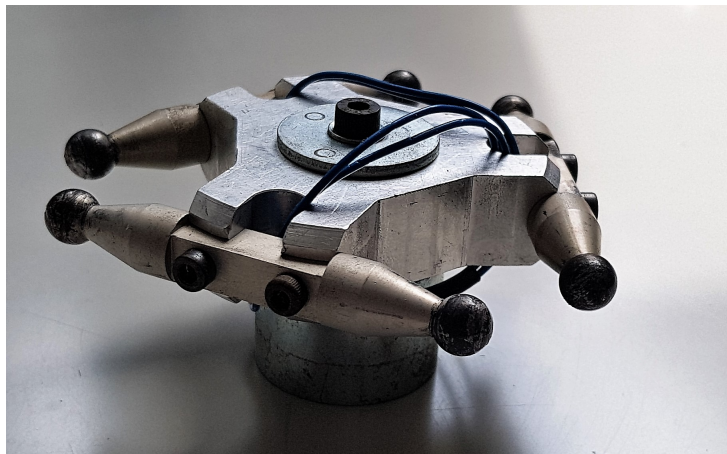


Figure 1.12. Mobile platform



1.2 The control system

The Delta robot is a multiple input multiple output (MIMO) system. In fact the control system, at each iteration, acquires the data of the position of each motor by means of encoders and then provides the right torque for each actuator, in order to reach the desired angular position. Let us consider the simple example of a proportional controller reported in equation 1.1. It is shown that the matrix of the gains is diagonal and with constant

value. In this way it is possible to control each motor individually as if it was a single input single output system (SISO).

$$\begin{bmatrix} \tau_1 \\ \tau_2 \\ \tau_3 \end{bmatrix} = K_p \begin{bmatrix} 1 & 0 & 0 \\ 0 & 1 & 0 \\ 0 & 0 & 1 \end{bmatrix} \begin{bmatrix} e_1 \\ e_2 \\ e_3 \end{bmatrix} \quad (1.1)$$

where τ_i is the torque applied at the i^{th} motor and e_i is the angular position error. Because of that, the system can be considered as three separate SISO systems that can be controlled independently (Equation 1.2).

$$\tau_i = K_p e_i \quad (1.2)$$

where $i = 1,2,3$ is the motor taken into consideration. For sake of simplicity of the notation, from now on all the equations are reported only in case of a single motor and not in the matrix form.

The control system of this direct drive Delta robot, has been developed using C++ language via Visual Studio software from Microsoft. The real time communication has been implemented using Windows XP equipped with RTX extension. The PC is equipped with a dual core E7300 2.66GHz CPU and 2Go of DDR2 memory. The HAL timer period of the RTX extension is set at 100 μs while the sampling frequency varies between 1 kHz and 2 kHz depending on the experiment performed.

The trajectories have been designed using FlexWare, an integrated environment for developing robotic applications. The FlexLanguage is a C-like interpreted language. FlexWare has various trajectories predefined (such as the straight line and the half-elliptic trajectory between two points) defined in the task space and automatically converted in joint coordinates. Flexware is the tool responsible of computing the inverse kinematic because the control system operates in joint space. The uncertainty of each measurement performed in this test is $\delta = 0.0008$ mm and in order to lighten the notation it will not be repeated.

1.3 Dynamic model

The dynamic model of a robot describes the relationship between the torque applied to the actuated joints and the movement of the end effector in the workspace. Two different dynamic models can be defined:

- Direct dynamic model
- Inverse dynamic model

The former expresses the movement of the end effector with respect to the torque applied to the motors, while the latter defines the torque necessary to obtain a certain trajectory of the end effector in the workspace. Since the purpose of this chapter is to define the model to be used in order to apply the feedforward torque, only the inverse dynamic model will be taken into consideration.

The inverse dynamic model expresses the torque that each motor has to provide in order to obtain the desired displacement of the end effector. The expression of the torques is not linear and it depends on the joint position q_d , velocity \dot{q}_d and acceleration \ddot{q}_d . When talking

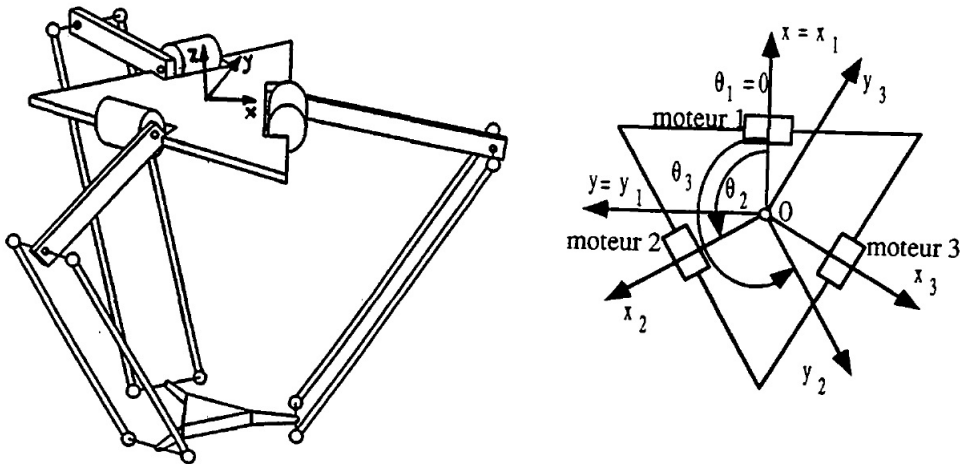
about feedforward torque, all the variables are the desired ones and not the measured ones. In this way their variation is smoother and, since the trajectory is known a-priori, it is possible to evaluate the torque off-line, reducing the computational effort.

The parallel structure of the Delta robot makes difficult to obtain its dynamic model because of the interdependence of the joint variables. Various techniques have been used to define the model, the one used in this text has been developed by A. Codourey [8] and it is based on the parametrisation of the system and the reference frames. The following paragraphs report a brief summary of his work.

The Delta robot schematic is shown in figure 1.13, thanks to its ternary symmetry it is possible to consider each kinematic chain independently and assign to it a reference frame. The reference of the base $R(O, x, y, z)$ is placed at the centre of the fixed base, with the z axis perpendicular to the plane where the base lays, x axis is orthogonal to the rotation axis of a motor. The three reference frames of the kinematic chains $R_i(O_i, x_i, y_i, z_i)$ have the same z axis and origin, axes x and y are obtained by means of a rotation of θ_i around the z axis of the fixed base. The first reference frame of the three chains coincides with the one of the base; the second and the third reference frame are obtained rotating the first one around the z axis of the fixed base of angles such that their x axis is perpendicular to the rotation axis of the other two motors (conventionally the Delta robot is assembled in a way that the two angles are of 60° and 120° with respect to the fixed frame R). The following matrix R_i describes the relation between two reference frames:

$$R_i = \begin{bmatrix} \cos(\theta_i) & \sin(\theta_i) & 0 \\ -\sin(\theta_i) & \cos(\theta_i) & 0 \\ 0 & 0 & 1 \end{bmatrix} \quad (1.3)$$

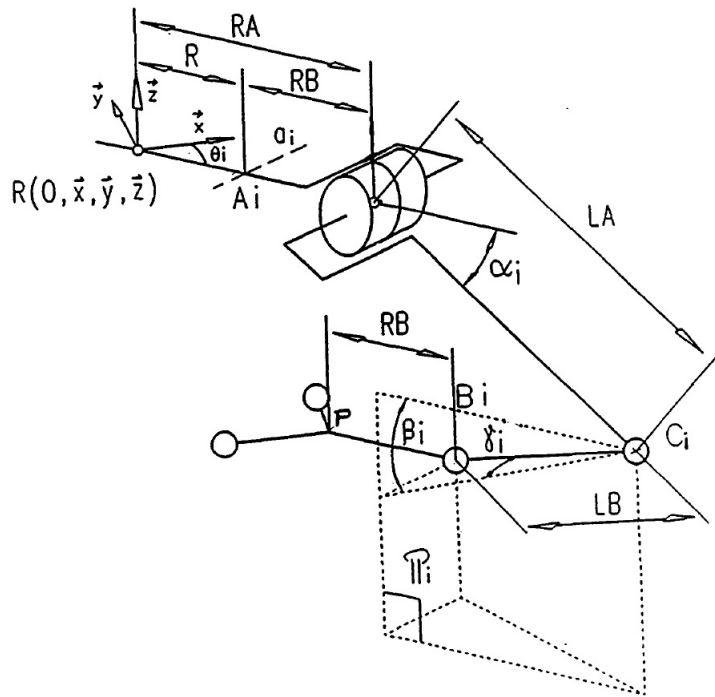
Figure 1.13. Delta 3DoF and its reference systems. Image taken from [8]



Considering each kinematic chain individually (Figure 1.14), the following geometric parameters are defined

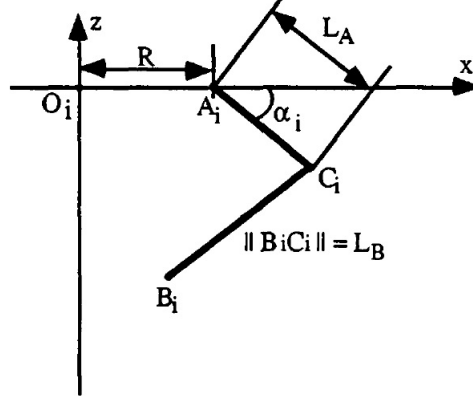
- R_A : distance between the centre of the base and the rotation axis of the motor
- R_B : distance between the centre of the mobile platform and the forearm
- L_A : length of the arm
- L_B : length of the forearm
- $R = R_A - R_B$
- α_i : angle between the arm and the fixed base plane
- β_i : angle between the forearm and a plane parallel to the fixed base
- γ_i : angle between the forearm and a plane orthogonal to the fixed base

Figure 1.14. Geometric parameters of a single chain. Image taken from [8]



Taking into account all the elements of the Delta robot is not feasible since it creates a system too complex to be solved in real time. Because of that, some simplifications have been made such as neglecting all the frictions, neglecting the inertia of the forearms and considering their mass split between the elbow (end of the arm) and the mobile platform. Thanks to these assumptions, the parallelogram structure of the forearms can be considered as a massless link (Figure 1.15) and the computational effort is compatible with real time constraints.

Figure 1.15. Kinematic chain. Image taken from [8]



Thanks to the simplifying assumptions it is possible to isolate the mobile platform and consider it independently. The bonding forces between it and the three forearms can be defined by means of the Newton equation obtaining

$$-\sum_{i=1}^3 F_i + G_n = m_n \cdot \ddot{X} \quad (1.4)$$

with F_i the force between the mobile platform and the forearm, G_n the gravity force acting on the mobile platform, m_n mass of the mobile platform including the contribution of the forearm, \ddot{X} the acceleration of the mobile platform in the reference frame R . Since the forearm is considered massless, the force applied by the mobile platform is equal and opposite to the one applied by the arm, the direction of those forces is the forearm (Figure 1.15).

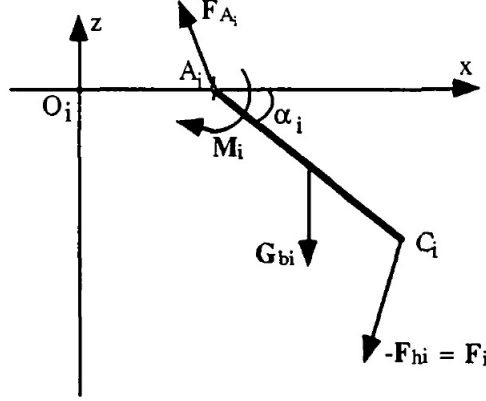
$$B_i C_i = B_i O_i + O_i A_i + A_i C_i \quad (1.5)$$

Knowing the direction of the forces F_i it is possible to obtain their norm.

$$F_i = |F_i| \frac{B_i C_i}{|B_i C_i|} \quad (1.6)$$

Substituting 1.6 in 1.4 a system with three unknowns is obtained, F_1 , F_2 and F_3 . All the forces are defined both in norm and direction.

Figure 1.16. Forces acting on the arm. Image taken from [8]



Considering the reference frame R_i of the i^{th} arm, using the Euler equation it is possible to obtain the torque of the single motor

$$M_i + A_i C_i \wedge F_i + r_{A_i G_{bi}} \wedge G_{bi} = I_{bi} \ddot{\alpha}_i \quad (1.7)$$

with M_i the torque around A_i , $r_{A_i G_{bi}}$ is the position of the centre of gravity of the i^{th} arm, G_{bi} is the gravity force acting on the arm with respect to the reference frame R_i , I_{bi} is the moment of inertia of the i^{th} arm around A_i and $\ddot{\alpha}_i$ is the acceleration of the i^{th} arm.

Considering the reference frame of figure 1.16, the torque is applied along the y axis with positive direction defined according to the right-hand rule. The resolution of the equation for the y component gives the equation 1.8:

$$M_{y_i} = I_{by_i} \ddot{\alpha}_i - F_i \frac{L_A}{L_B} [z_i \cos \alpha_i - (R - x_i) \sin \alpha_i] - r_{G_b} m_b g \cos \alpha_i \quad (1.8)$$

with g the gravitational acceleration, m_b total mass of the arm comprehensive of the part of the forearm, x_i and z_i the coordinates of the mobile platform in R_i . The dynamic model is function of the angular acceleration of each arm and also of the acceleration of the mobile platform in a non linear way.

Chapter 2

PID controller and resonance frequency

All the considerations made in the previous chapter are valid only in case of rigid bodies. This assumptions are generally true but when the performances are pushed to the limit, the robot stops behaving like a rigid body and it starts vibrating at its natural frequency. The objective of this chapter is to identify the resonance frequency of the different arms with whom the robot can be assembled and remove it by means of a notch filter. In order to do that, the PID controller has been used to control the robot.

2.1 The PID controller

The proportional-integral-derivative (PID) controller is one of the most commonly used control loop feedback mechanism, especially in industrial applications. In fact it can be tuned directly on the system by trial and error, without the necessity of having a mathematical model. Moreover it is able to compensate various disturbances such as the static error, thanks to the integral component, and the gravity effects, thanks to the derivative one.

Since the robot is controlled in position, the signal entering into the controller is the position tracking error $e(t)$ that is the difference between the desired position and the measured position of the motors. The equation 2.1 represents the transfer function of the PID controller:

$$\tau(t) = K_p e(t) + K_d \frac{de(t)}{dt} + K_I \int_0^t e(t') dt' \quad (2.1)$$

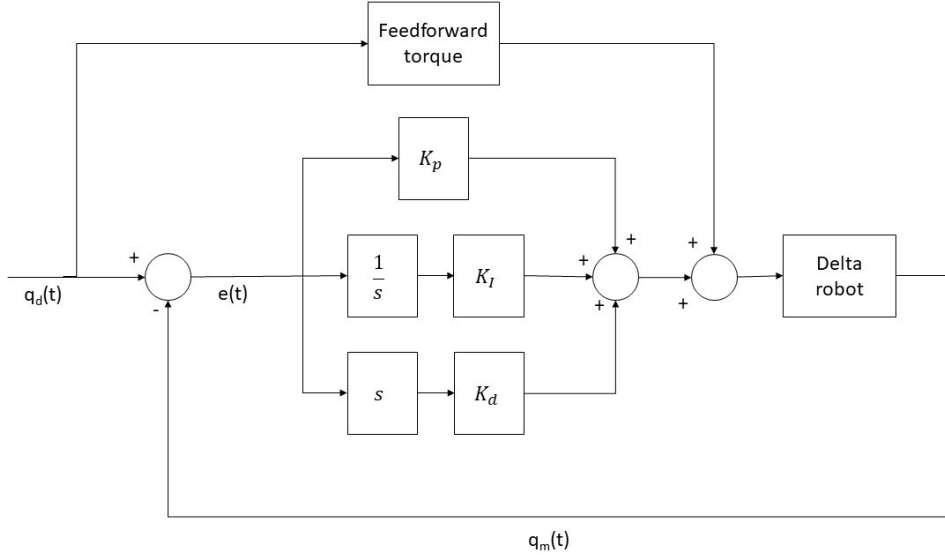
where $\tau(t)$ is the torque applied to the motor, $e(t) = q_d(t) - q_m(t)$ with $q_d(t)$ the desired position of the motor at time t and $q_m(t)$ the measured position, K_p , K_d and K_I are the control parameters. The velocity error has been evaluated numerically, considering the variation of the error in two sampling periods.

$$\frac{de(t)}{dt} = \dot{e}(t) = \frac{e(t) - e(t - 2)}{2T_s} \quad (2.2)$$

where T_s is the sampling period, $e(t)$ is the error evaluated at time t and $e(t - 2)$ is the error evaluated two sampling periods before. The choice of using two sampling periods

has been made in order to have a smoother variation of the velocity. In this way, in fact, the high frequency oscillations are filtered. The figure 2.1 shows the control loop used to control the robot.

Figure 2.1. PID controller block scheme



The controller has been tuned directly on the robot, without any previous simulation. The control parameters have been found by trial and error, increasing the proportional gain K_p until the system started oscillating, then increasing the derivative parameter K_d in order to reduce the oscillations. Once reached the best dynamic performances, the integral gain K_I has been increased to compensate the static error.

2.2 Effect of the feedforward torque

Once the inverse dynamic model has been implemented, some preliminary tests have been performed with the intent of evaluating the effect of the feedforward torque, in terms of reduction of errors [13]. In this case in order to consider the manipulator as made of rigid bodies, the controller has been tuned with the intent to avoid exciting the resonance frequency.

The trajectory applied in these tests consists in moving the mobile platform in the workspace by means of semi-elliptic arches with an acceleration of 2.5 G. Five different types of feedforward torque have been applied:

- No compensating torque
- Compensation of the inertia of the motor
- Compensation of the inertia of the motor and the inertia of the arm
- Compensation of the inertia of the motor, inertia of the arm and gravity of the arm. (2/3 of the forearms weight are included with the elbow)

- Complete model: compensation of the inertia of the motor, inertia of the arm, gravity of the arm and effects of the mobile platform.

Performances have been evaluated comparing the root mean square error (RMSE) (eq. 2.3) and the peak errors (eq. 2.4) between the desired position of the mobile platform and the measured one. The position of the mobile platform is not measured directly, as a matter of fact the angular position of the motors is measured by means of encoders. The Cartesian coordinates of the end effector are obtained applying the direct kinematic model to the measured angles. The great rigidity and lightness of the structure does not allow any significant bending of the links, permitting the direct kinematic model to be used without spoiling the accuracy of the measurements.

$$RMSE = \sqrt{\frac{1}{N} \sum_{k=1}^N (e_x^2(k) + e_y^2(k) + e_z^2(k))} \quad (2.3)$$

$$peak_{x,y,z} = \max(|e_{x,y,z}|) \quad (2.4)$$

The robot was assembled with carbon fibre arms, WPS forearms and mobile platform without the magnet attached to it. No transported payload is present. The robot is controlled by means of a PID controller. The results obtained are reported in tables 2.1 and 2.2. The last column of table 2.1 reports the improvement of the RMSE when each a-priori torque is applied with respect to the case when none is present (first line of the table). In table 2.2 it can be observed a considerable reduction of the peak errors, especially for axes x and y .

The improvements of the performances applying compensating torques with different levels of precision are not negligible and that is why, for all the following measurements, the complete feedforward model has been used to establish the compensating torque, since it is the one that gives better results.

Table 2.1. Cartesian RMSE - Acceleration 2.5 G - No mass transported

Type of compensating torque	RMSE [mm]	Improvement RMSE[%]
No a-priori torque	0.2295	-
Motor inertia	0.1498	34.73
Arm inertia	0.1008	56.08
Arm inertia & gravity	0.0912	60.26
Complete model	0.0771	66.41

Table 2.2. Cartesian peak errors [mm] - Acceleration 2.5 G - No mass transported

Axis	No a-priori torque	Motor inertia	Arm inertia	Arm inertia & gravity	Complete model
x	0.4691	0.2940	0.1995	0.1813	0.1267
y	0.8235	0.5736	0.3639	0.3348	0.2159
z	0.2523	0.1437	0.1176	0.1004	0.0999

2.3 Resonance frequency

In order to obtain even better results, a special attention has to be given to the resonance frequency. The technique used to find it consisted in increasing the gains (especially proportional and derivative ones) of the PID controller until the robot started vibrating and making noise but still remaining controllable. Once reached this limit, the resonance frequency has been found comparing the results obtained by a Spectrum Analyser and the Fast Fourier Transform (FFT) of the angular velocity of the motors. The Spectrum Analyser is an Application for Smartphone, able to derive the frequency by recording the noise emitted by the robot (Figure 2.2), while the FFT has been executed on MATLAB®. In figure 2.3 is reported the FFT of the error velocity in case of aluminium arm. Two peaks are present, one at low frequency and one at around 360 Hz. The former is due to the controller, while the latter shows the natural frequency of the robot assembled with aluminium arms. It has also been observed that changing the position of the mobile platform in the workspace causes a variation of the value of the resonance frequency of the manipulator, the second peak in fact is not a single line but has a triangular shape. This fact can be clearly noticed in figure 2.4 where the resonance frequencies of the different positions reached by the robot during the task are reported in different colors. Because of the wide range of frequencies, a band stop filter has been designed instead of a notch one. In this way it was possible to take into consideration and eliminate all the possible frequencies that can be excited using a single filter. Moreover the second peak corresponds to the one recorded by the spectrum analyser. It has also been observed that the vibrations due to the frequency are definitely more present in the velocity error than in the position one and because of that only the former has been filtered. The designed filter is digital and it is applied in the control loop before the derivative gain. The structure of the filter applied is reported in equation 2.5:

$$y(t) = \frac{B_0u(t) + B_1u(t - 1) + B_2u(t - 2)}{1 + A_1y(t - 1) + A_2y(t - 2)} \quad (2.5)$$

The presence of the filter allows to increase the gains of the controllers previously found without exciting the resonance frequency and so improving the performances of the robot. The sampling frequency used to perform this task is 2 kHz and the HAL timer is set to 100 μ s. The frequencies cut by the filter are reported in table 2.3, according to the arms mounted on the robot.

Table 2.3. Resonance frequencies of the robot depending on the arm material

Arm material	Aluminium	Carbon fibre
Frequency	356-368 Hz	490-500 Hz

The range of frequencies is so wide because it has been considered also the case when a mass is transported. The increment of weight of the mobile platform, in fact, affects the value of the resonance frequency, reducing it. In figure 2.5 is depicted the schematic of the control loop after inserting the filter.

Figure 2.2. Aluminium arms spectrum analysis

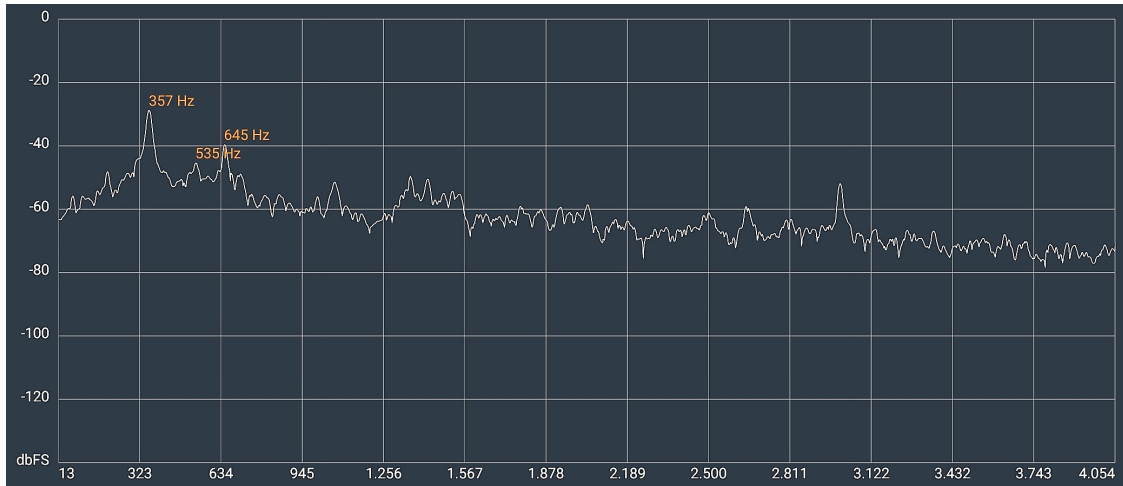


Figure 2.3. Aluminium arms FFT

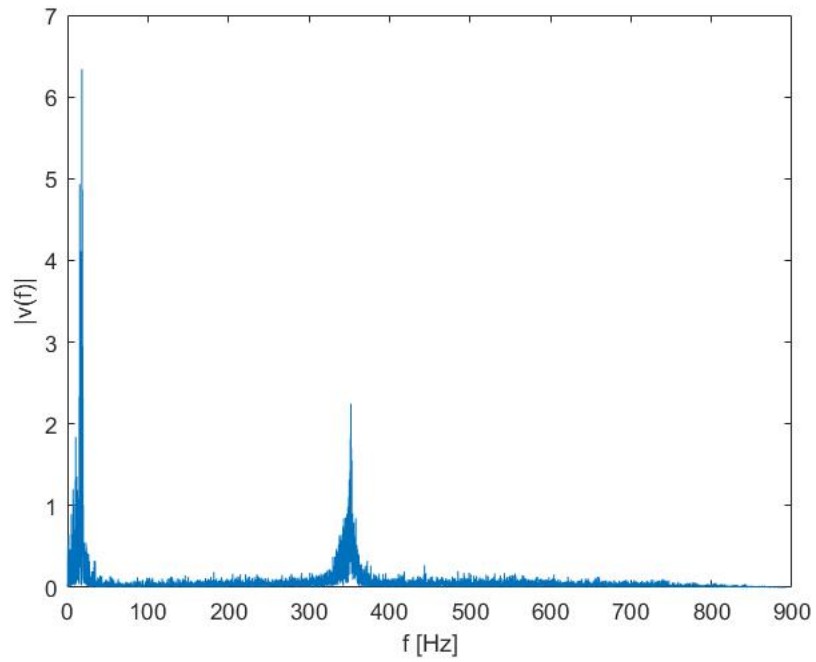


Figure 2.4. Aluminium arms resonance frequencies according to mobile platform position in space

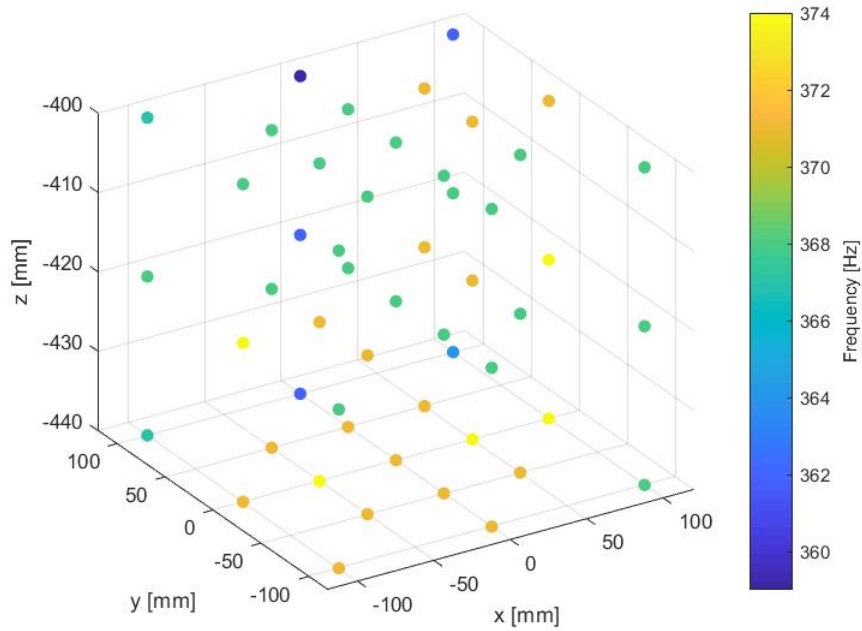
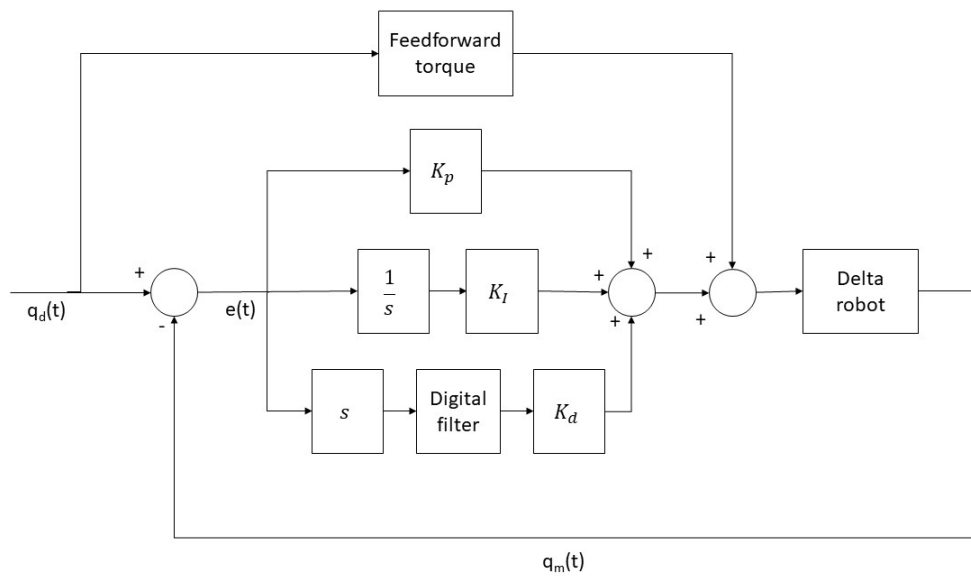


Figure 2.5. PID controller block scheme with digital filter



All the different parts available have been tested and for each configuration arm-forearm a specific PID controller has been tuned. The value of the gains is reported in tables 2.4 and 2.5. The higher resonance frequency of the carbon fibre arms allows to have higher gains with respect to those available with the aluminium arms. In fact in order to excite an higher frequency, higher gains are required.

Table 2.4. Aluminium arm - PID control parameters - sampling frequency 2 kHz

Forearms	K_p	K_d	K_I
WPS	2.4	0.019	80
BAC	3.0	0.021	80
GAS	2.7	0.024	80

Table 2.5. Carbon fibre arm - PID control parameters - sampling frequency 2 kHz

Forearms	K_p	K_d	K_I
WPS	5.5	0.017	90
BAC	5.0	0.025	90
GAS	7.0	0.025	90

2.4 Performance comparison between arms

Once tuned the controller for each combination of arm-forearm, the performances have been evaluated and compared. The test has been performed in the following way. The mobile platform moves in the workspace freely, without any transported mass (no-load condition). The dynamic model of the robot is exactly known and the feedforward torque is applied. The trajectory of the end effector used to test the various configurations is a typical trajectory used in pick-and-place operations, with semi-elliptic arches between the points of pick and place (best one according to [8]), as shown in pictures 2.6 and 2.7. The acceleration is 2.5 G and the jerk time is 0.01 s.

Figure 2.6. 3D trajectory

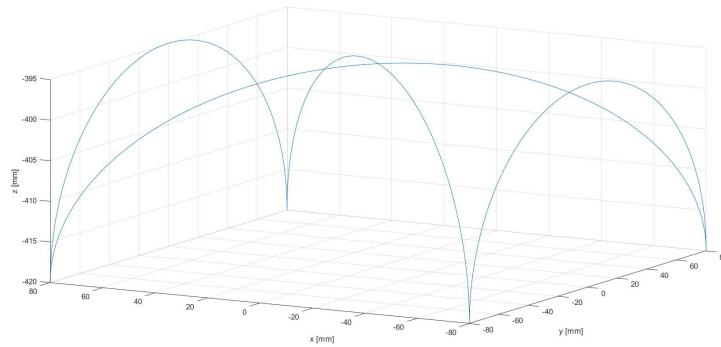
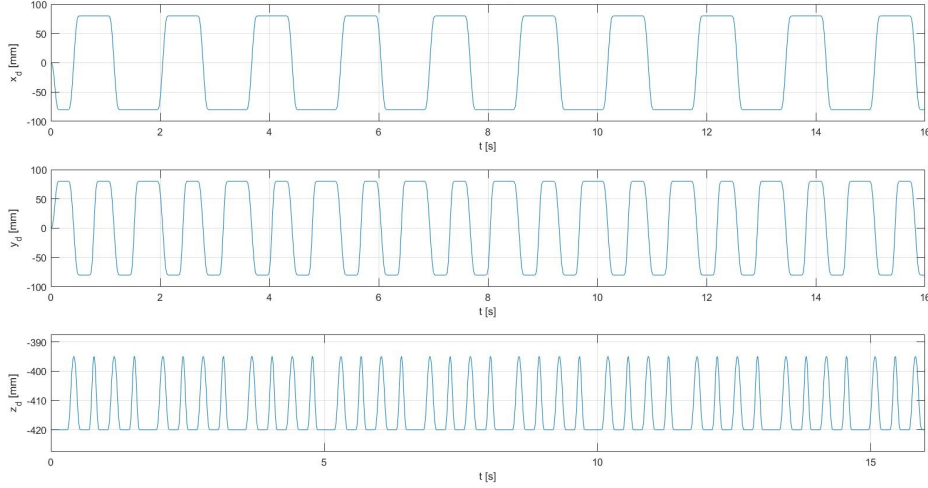


Figure 2.7. Cartesian variables - Acceleration 2.5 G



The performances have been evaluated comparing the plot of the Cartesian error, the root mean square error (RMSE) (Equation 2.3) and the peak errors (Equation 2.4) of the mobile platform position. The figures 2.8, 2.9 and 2.10 represent the Cartesian error for all the duration of the movement. Last two seconds are zoomed in order to provide a more clear view of the situation (Figures 2.11, 2.12 and 2.13).

It can be easily observed that, independently from the forearm, the carbon fibre arm has better performances than the aluminium one. Both RMSE and peak errors are always smaller when the carbon fibre arms are mounted on the robot (Tables 2.6, 2.7 and 2.8). The last two columns of table 2.6 report the improvement in terms of RMSE between the aluminium arms and the carbon fibre ones. This fact is due to the possibility to have higher control gains without exciting the resonance frequency thanks to the greater rigidity of the carbon fibre arms. Also the forearms affect slightly the performances, in fact it can be noticed that the best results are obtained using the WPS forearms.

Table 2.6. RMSE - Acceleration 2.5 G - No mass transported

Forearms	Aluminium arm		Carbon fibre arm		Improvement %	
	Joint [Deg]	Cartesian [mm]	Joint [Deg]	Cartesian [mm]	Joint	Cartesian
WPS	0.0729	0.2794	0.0325	0.1222	44.65	43.74
BAC	0.0756	0.2962	0.0382	0.1450	50.45	48.96
GAS	0.0895	0.3511	0.0424	0.1607	47.37	45.78

Table 2.7. Joint space peak errors - Acceleration 2.5 G - No mass transported

Joint	Aluminium arms [Deg]			Carbon fibre arms [Deg]		
	WPS	BAC	GAS	WPS	BAC	GAS
1	0.1120	0.1108	0.1306	0.0547	0.0497	0.0665
2	0.2064	0.2386	0.2794	0.0967	0.0976	0.1234
3	0.1119	0.1357	0.1472	0.0719	0.0871	0.0886

Table 2.8. Cartesian space peak errors - Acceleration 2.5 G - No mass transported

Axis	Aluminium arms [Deg]			Carbon fibre arms [Deg]		
	WPS	BAC	GAS	WPS	BAC	GAS
x	0.5638	0.5425	0.6221	0.2181	0.1862	0.2825
y	0.7537	0.9670	1.1721	0.2867	0.3442	0.3710
z	0.4548	0.4567	0.5574	0.2827	0.3032	0.3623

Figure 2.8. Forearms with peek coupling and spherical socket (WPS) - Acceleration 2.5 G - No mass transported

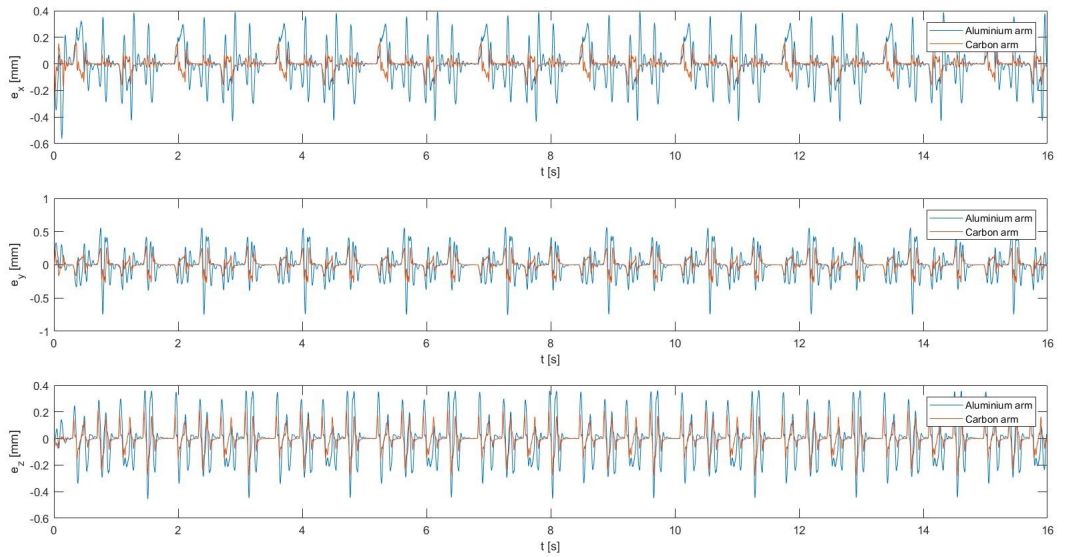


Figure 2.9. Forearms with aluminium coupling and conical socket (BAC) - Acceleration 2.5 G - No mass transported

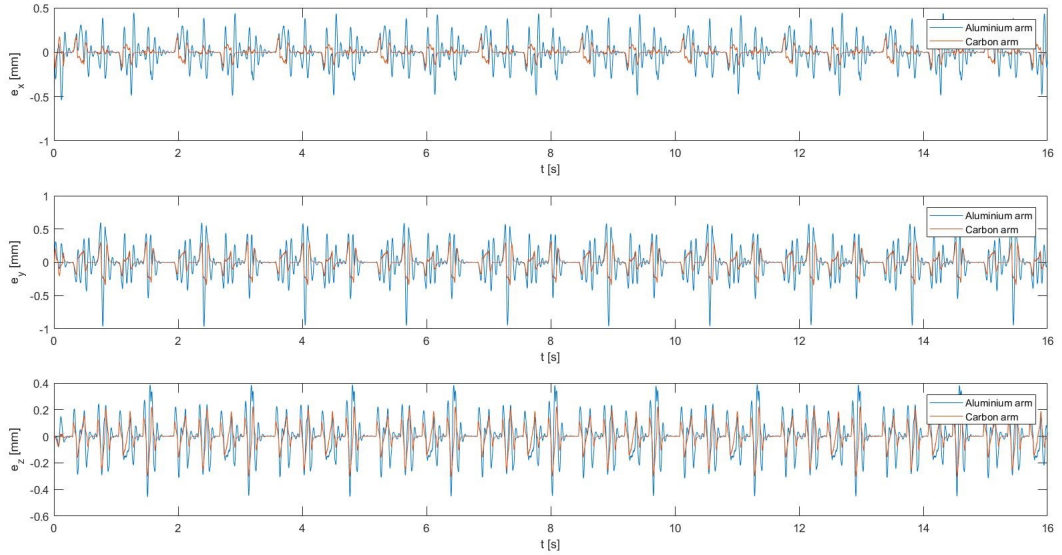


Figure 2.10. Forearms with aluminium coupling and spherical socket (GAS) - Acceleration 2.5 G - No mass transported

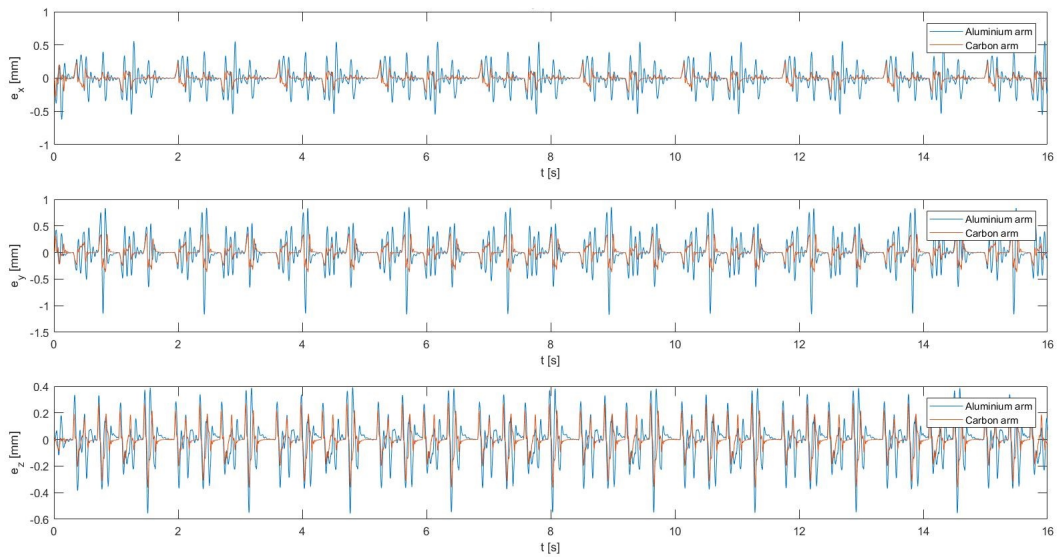


Figure 2.11. Forearms with peek coupling and spherical socket (WPS) - Acceleration 2.5 G - No mass transported

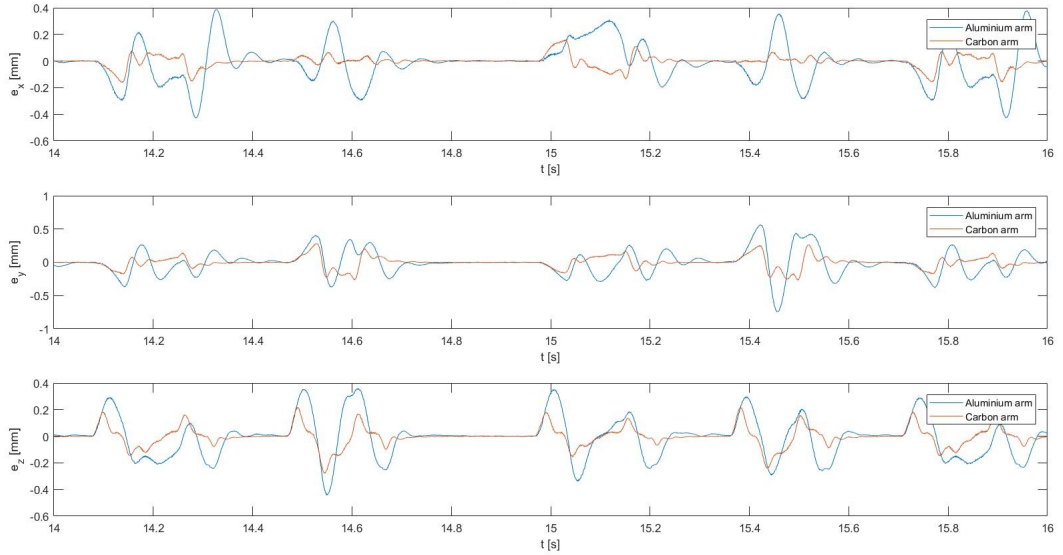


Figure 2.12. Forearms with aluminium coupling and conical socket (BAC) - Acceleration 2.5 G - No mass transported

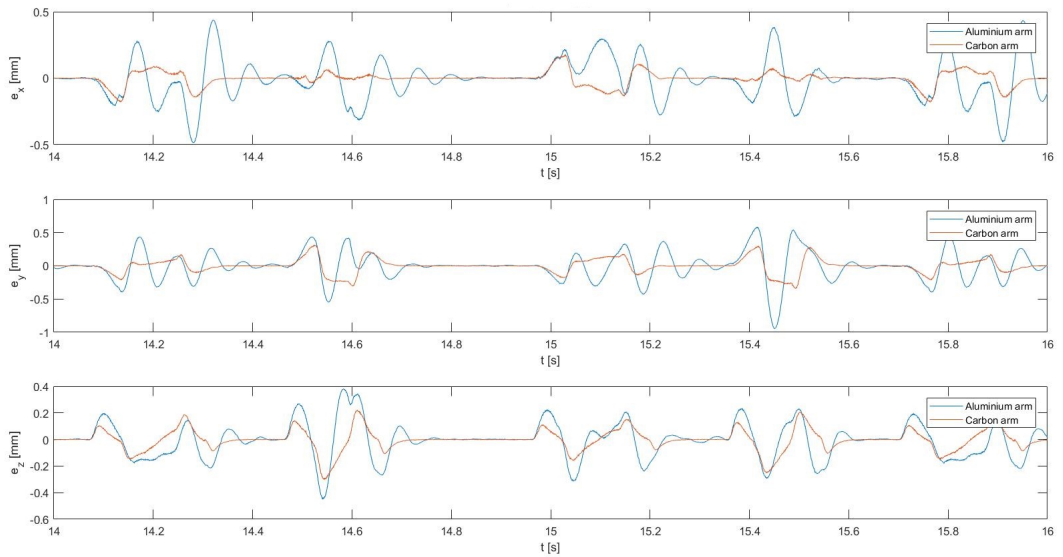
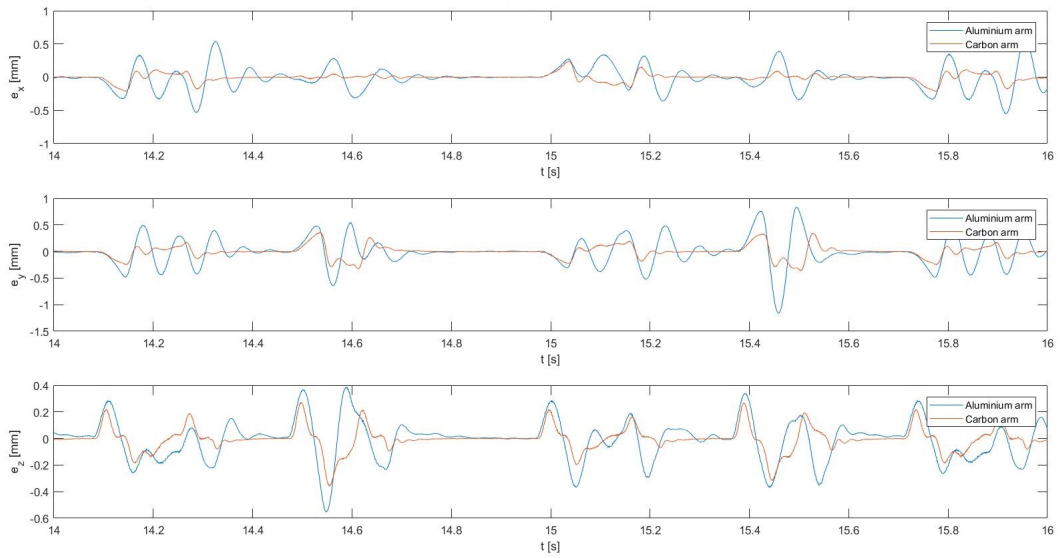


Figure 2.13. Forearms with aluminium coupling and spherical socket (GAS) - Acceleration 2.5 G - No mass transported



Chapter 3

RISE and Adaptive RISE controllers

3.1 Structure of the RISE controller

The robust integral of signum of error (RISE) controller, is a recently developed technique of robust control [16]. One of the main advantages of the RISE controller is the fact that it is able to compensate a remarkable class of uncertainties without any, or at least a very small, knowledge of the system to be controlled. In mechanical manipulators the number of uncertainties is not negligible at all, in fact the dynamics of the robot themselves present a lot of uncertainties and also the external environment contributes to increase the number of uncertainties since it is not possible to model it exactly.

Desired joint position, velocity and acceleration are denoted respectively by $q_d(t)$, $\dot{q}_d(t)$ and $\ddot{q}_d(t)$. The combined error $r(t)$ (Equation 3.1) is then defined combining the velocity-position tracking error

$$r(t) = \dot{e}(t) + \alpha_1 e(t) \quad (3.1)$$

where $e(t) = q_d(t) - q_m(t)$, given $q_m(t)$ the measured position and α_1 a control design gain. Then the auxiliary error $\nu(t)$ (equation 3.2) is defined as

$$\nu(t) = \dot{r}(t) + \alpha_2 r(t) \quad (3.2)$$

where α_2 is another control design parameter. As well explained in [2] and [16] the RISE feedback control law is given by

$$\tau_{RISE}(t) = (k_s + 1)r(t) - (k_s + 1)r(t_0) + \int_{t_0}^t [(k_s + 1)\alpha_2 r(\tau) + \beta \text{sgn}(r(\tau))] d\tau \quad (3.3)$$

where k_s and β are the last two control design parameters. Detailed proof of the stability can be found in [2]. The control system is stable if $\alpha_1 > 0.5$, $\alpha_2 > 1$ and k_s large enough to guarantee the performance without compromising the stability.

As stated in [13], a model-based feedforward term can increase the tracking performance. Because of that, the following augmented control law has been used

$$\tau(t) = \tau_{RISE}(t) + Y_d(q_d, \dot{q}_d, \ddot{q}_d)\theta_0 \quad (3.4)$$

where Y_d is the regression matrix which is a non-linear function of the desired joint positions, velocities and accelerations, and θ_0 is the vector containing the best estimation of the manipulator's geometric and dynamic parameters. The majority of these parameters do not vary during the robot's activities, but in case of pick-and-place operation of unknown payloads, the mass of the mobile platform changes. In order to compensate this change, an adaptive feedforward term has been designed by M. Bennehar [2], where the nominal parameter vector θ_0 is replaced by the estimated one $\hat{\theta}_0$

$$\tau(t) = \tau_{RISE}(t) + Y_d(q_d, \dot{q}_d, \ddot{q}_d)\hat{\theta}_0 \quad (3.5)$$

The estimated parameter $\hat{\theta}_0$ is updated following the adaptation law:

$$\hat{\theta}_i(t) = \begin{cases} \gamma_i \phi_i & , \text{ if } -\theta_{b_i} < \hat{\theta}_i < \theta_{b_i} \text{ or } \hat{\theta}_i \leq \theta_{b_i} \text{ and } \phi_i \leq 0 \text{ or } \hat{\theta}_i \leq -\theta_{b_i} \text{ and } \phi_i \geq 0 \\ 0 & , \text{ if } \hat{\theta}_i \geq \theta_{b_i} \text{ and } \phi_i \geq 0 \text{ or } \hat{\theta}_i \leq -\theta_{b_i} \text{ and } \phi_i \leq 0 \end{cases} \quad (3.6)$$

where $\hat{\theta}_i$ is the estimate of the unknown parameter θ_i ; γ_i is the i^{th} element of the diagonal adaptation matrix Γ ; ϕ_i is the i^{th} element of the vector $\phi = Y_d^T(\cdot)r(t)$; θ_{b_i} is the bound of the estimated parameter.

The adaptation law 3.6 guarantees that the estimated parameters remain in the range given by the upper and lower bounds, while the adaptation mechanism estimates the parameters in real time and makes them available to the feedforward term. The structure of the adaptation law is very simple since it is based only on the regression matrix and the combined position-velocity error, and because of that it suits for real-time implementations. The stability proof of the controller is reported in [2] and it shows that the joint position tracking error $e(t)$ goes to zero as time goes to infinity. Two Adaptive-RISE controllers have been used, the first one able to estimate the mass of the transported payload, the second used to estimate the inertia of the arms.

3.2 Estimation of the transported mass

The first of the two versions of the Adaptive RISE (A-RISE) controller tries to estimate the mass of the payload on-line. The code of the controller has been developed by Bennehar[2] and slight modifications have been made. In fact in [2] the controller tries to estimate the mass of both mobile platform and payload combined, while in the following examples the mass of the mobile platform is already known and used in the feedforward term $\tau_{FF}(t)$, that is structured as follows:

$$\tau_{FF}(t) = I_{tot}\ddot{q}_d(t) - \cos(\alpha) \left(\frac{L_{arm}}{2} m_{arm} + L_{arm} m_{elb} \right) + \left(J^T G + J^T \ddot{X} \right) m_e \quad (3.7)$$

with $I_{tot} = I_{arm} + I_{mot} + I_{elb}$, where I_{arm} , I_{mot} and I_{elb} are respectively the inertia of the arm, the motor and the elbow; α is the angle between the arm and the base; L_{arm} is the length of the arm; m_{arm} is the mass of the arm; m_{elb} is the mass of the elbow and includes, thanks to the simplifications made, $2/3$ of the mass of the forearm; G is the gravity acceleration; J is the Jacobian matrix; \ddot{X} is the desired acceleration of the mobile platform in the Cartesian space; $m_e = m_p + m_t$ is the estimated mass, with m_p the mass of the mobile platform and m_t the transported mass estimated as

$$m_t(t) = m_t(t-1) + \Gamma \dot{m}_t(t) \quad (3.8)$$

with $\dot{m}_t(t) = Y_d^T(\cdot)r(t)$. In case of normal RISE, the feedforward torque applied is the same as 3.7 but with the difference that m_e is fixed, does not change in time, and its value is the mass of the mobile platform, m_p . Block schemes of both RISE and A-RISE are reported in figures 3.1 and 3.2.

Figure 3.1. RISE controller block scheme

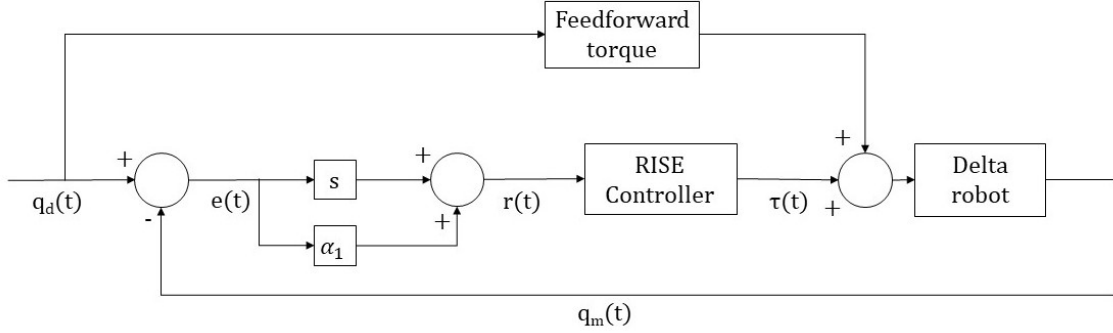
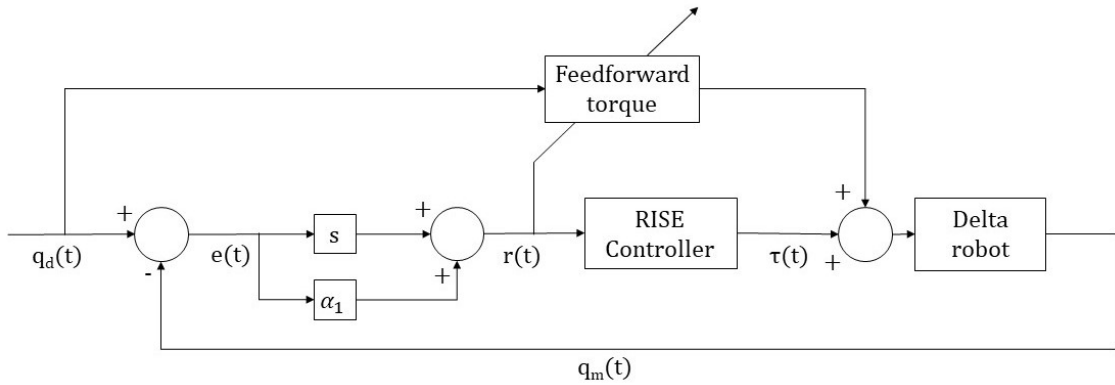


Figure 3.2. Adaptive RISE controller block scheme



In order to prove the quality of the controller and its ability to estimate on-line the value of the transported mass, all the configurations tried with the PID controller have been evaluated again, in the same conditions, but with this new controller. The trajectory applied, the filters, the sampling frequency and the HAL timer are all the same.

One of the main difficulty of the RISE controller is tuning properly the parameters. In fact it does not exist a general rule as in case of the PID controller [4]. The technique adopted to find the control parameters consisted in tuning the gains α_1 and α_2 in order to avoid oscillations, than increasing K_s until the vibrations started. β has been selected in order to reach a trade-off between the increase of oscillations and the reduction of the RMSE. The adaptive parameter Γ has been chosen in order to avoid big oscillations in the mass estimation but having at the same time a rapid estimate. In tables 3.1 and 3.2 are

listed all the tuning parameters of the controller in all the configurations tested. It can be noticed that the parameters of the different configurations tested vary considerably, in fact changing the forearms caused an unexpected variation in the control gains.

Table 3.1. Aluminium arm - RISE and A-RISE parameters - Sampling frequency 2 kHz

Forearm	α_1	α_2	K_s	β	Γ
WPS	400	1.35	0.15	3.0	0.2
BAC	400	1.66	0.30	2.0	0.2
GAS	200	7.00	0.40	2.0	0.2

Table 3.2. Carbon fibre arm - RISE and A-RISE parameters - Sampling frequency 2 kHz

Forearm	α_1	α_2	K_s	β	Γ
WPS	480	4.75	0.90	1.5	0.3
BAC	550	5.50	0.80	1.5	0.3
GAS	380	15.00	1.40	1.5	0.3

It can be noticed that either with carbon arms and with aluminium arms, the GAS forearms require a quite different controller with respect of the other two type of forearms. This fact can be attributed to both the sensitivity of the controller with respect to the inertia, and to the friction due to the ball and socket coupling of the elbow. In fact the GAS forearms are the heavier available and with the most wrapping socket, causing higher inertia and greater friction.

A first test to verify the capability of the controller has been performed moving the mobile platform freely in the workspace without any transported mass. But since all the parameters of the robot are already known in the feedforward torque, no difference has been observed between the RISE and the A-RISE controller and the estimated value of the transported mass is null, as expected.

In order to test the effectiveness of the A-RISE controller, a mass of 225 g has been attached to the mobile platform by means of a electric magnet but the control system is not aware of its presence. As stated before, the operating conditions are the same as when the PID controller has been tested. The mass of the payload is unknown to the system and so is not included into the dynamic parameters of the controller. It is expected that the A-RISE is able to estimate the value of the mass and use it in the feedforward torque, increasing the tracking performances while operating. The obtained results have been compared with those of the normal RISE. In the tables 3.3 and 3.6 are reported the RMSE of the various configurations tested, while in 3.4, 3.5, 3.7 and 3.8 the peak errors.

In this working situation the A-RISE, thanks to its ability of estimating the unknown mass and using it in the feedforward torque, gives better results than the original RISE. Those facts can be observed in the pictures 3.3, 3.4, 3.5 and 3.6 representing the trend of the Cartesian errors. When the A-RISE is present in the control loop, the oscillations of the errors are drastically reduced with respect to the normal RISE and their amplitude is lower. It is well evident that the carbon fibre arms give better results than the aluminium

ones. The improvements obtained using the A-RISE are due to the precision with whom the controller is able to estimate on-line the value of the transported mass. The trend of the mass estimation is shown in figure 3.7.

Table 3.3. Aluminium arm RMSE - Acceleration 2.5 G - 225 g mass transported

Forearm	RISE		A-RISE	
	Joint [Deg]	Cartesian [mm]	Joint [Deg]	Cartesian [mm]
WPS	0.1353	0.5513	0.0754	0.3065
BAC	0.1404	0.5742	0.0644	0.2615
GAS	0.2420	0.9807	0.0913	0.3632

Table 3.4. Aluminium arm joint space peak errors [Deg] - Acceleration 2.5 G - 225 g mass transported

Joint	RISE			A-RISE		
	WPS	BAC	GAS	WPS	BAC	GAS
1	0.2319	0.2080	0.3454	0.2316	0.1906	0.3064
2	0.3338	0.3283	0.5159	0.3003	0.2377	0.3718
3	0.3828	0.4220	0.4992	0.2495	0.2472	0.3046

Table 3.5. Aluminium arm task space peak errors [mm] - Acceleration 2.5 G - 225 g mass transported

Axis	RISE			A-RISE		
	WPS	BAC	GAS	WPS	BAC	GAS
x	1.1662	0.8800	1.5271	1.2039	0.8727	1.4771
y	1.9967	2.1011	2.9775	1.3378	1.2104	1.8214
z	0.6170	0.6268	0.9776	0.5592	0.3695	0.6044

Table 3.6. Carbon fibre arm RMSE - Acceleration 2.5 G - 225 g mass transported

Forearm	RISE		A-RISE	
	Joint [Deg]	Cartesian [mm]	Joint [Deg]	Cartesian [mm]
WPS	0.0790	0.3151	0.0357	0.1379
BAC	0.0837	0.3340	0.0352	0.1369
GAS	0.0800	0.3179	0.0352	0.1358

Table 3.7. Carbon fibre arm joint space errors [Deg] - Acceleration 2.5 G - 225 g mass transported

Joint	RISE			A-RISE		
	WPS	BAC	GAS	WPS	BAC	GAS
1	0.1445	0.1545	0.1231	0.1180	0.1077	0.1118
2	0.2057	0.2126	0.1714	0.1608	0.1710	0.1463
3	0.2052	0.2019	0.1863	0.0869	0.1069	0.1070

Table 3.8. Carbon fibre arm task space peak errors [mm] - Acceleration 2.5 G - 225 g mass transported

Axis	RISE			A-RISE		
	WPS	BAC	GAS	WPS	BAC	GAS
x	0.5779	0.5611	0.5490	0.5413	0.4805	0.5579
y	0.9592	0.9715	0.9491	0.5779	0.6082	0.6567
z	0.3455	0.4227	0.5056	0.3052	0.3449	0.3985

Figure 3.3. Aluminium arm - GAS forearms - Acceleration 2.5 G - 225 g mass transported

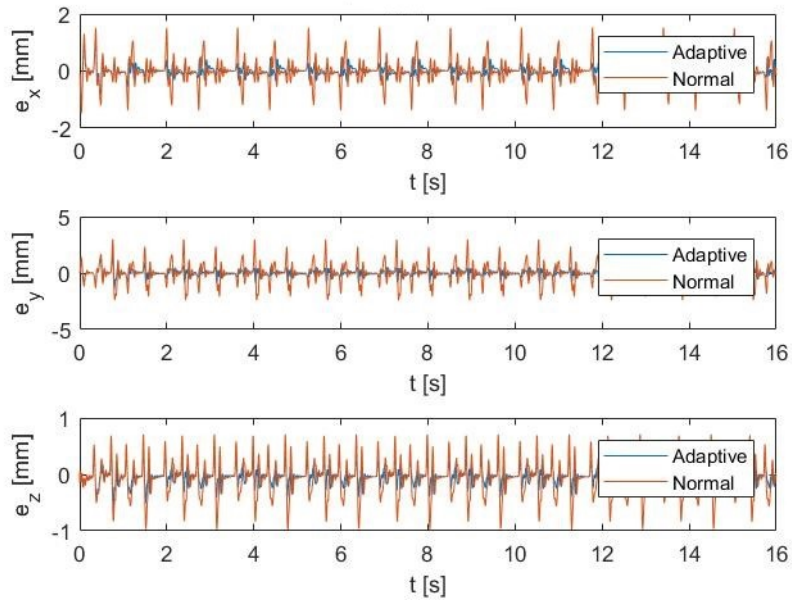


Figure 3.4. Aluminium arm - GAS forearms - 2 seconds zoom - Acceleration 2.5 G - 225 g mass transported

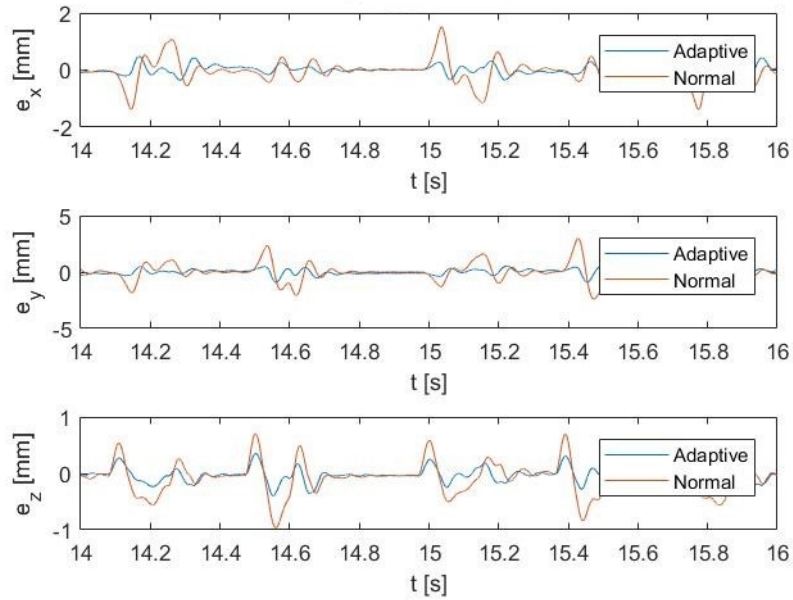


Figure 3.5. Carbon fibre arm - GAS forearms - Acceleration 2.5 G - 225 g mass transported

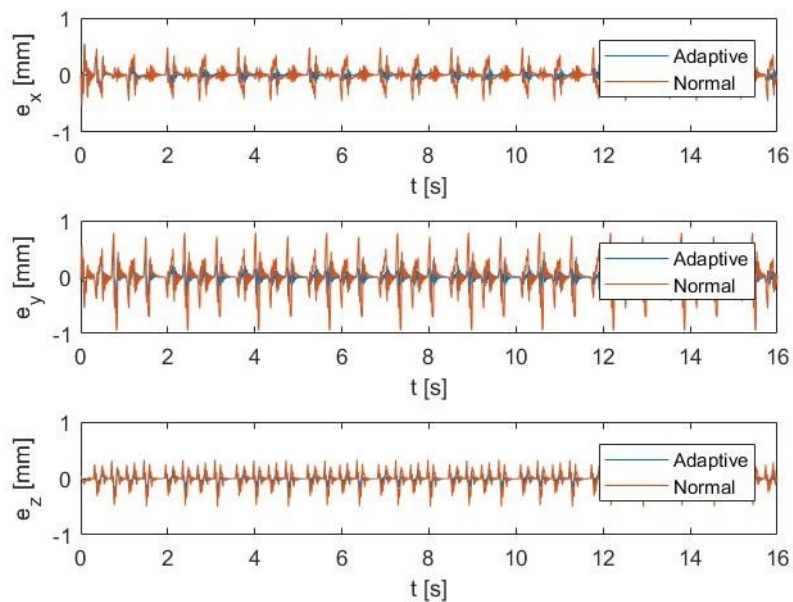


Figure 3.6. Carbon fibre arm - GAS forearms - 2 seconds zoom - Acceleration 2.5 G - 225 g mass transported

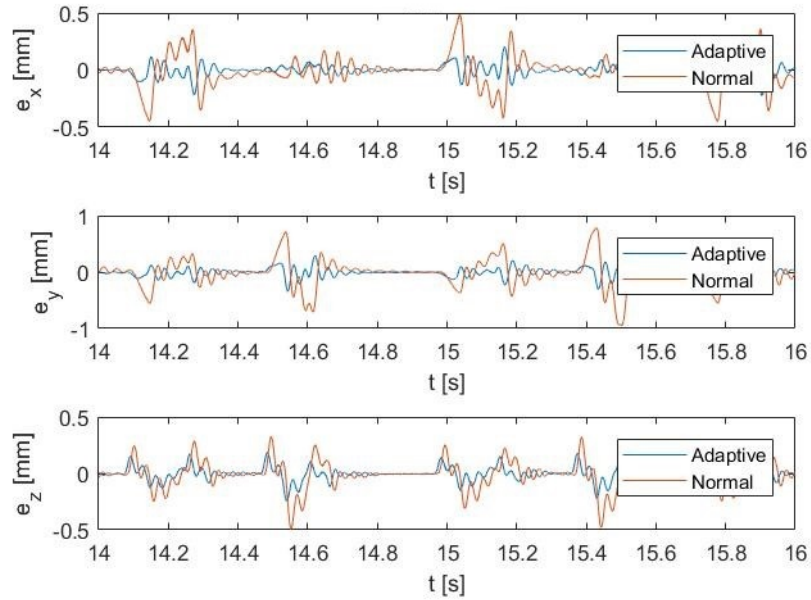
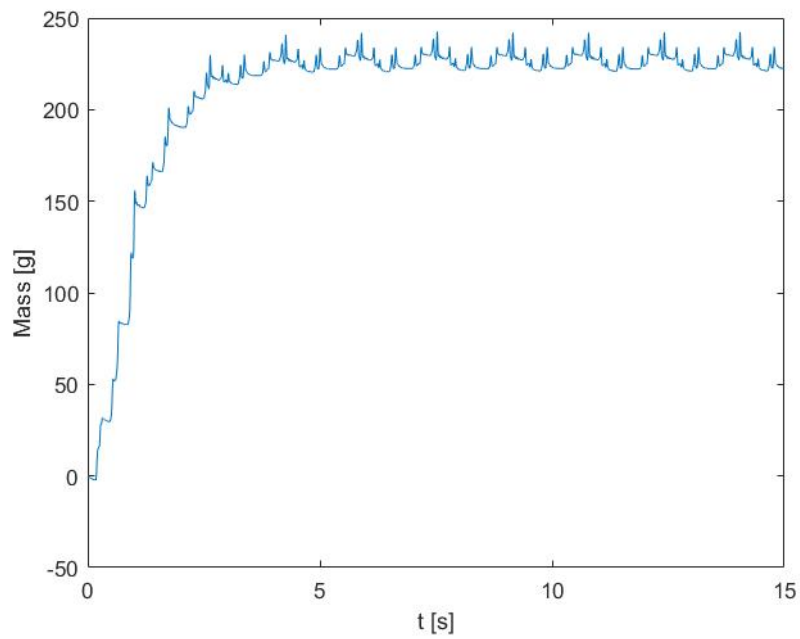


Figure 3.7. Transported mass estimation - Acceleration 2.5 G - 225 g mass transported



3.3 Estimation of the inertia of the arm

The analytical calculation of the inertia of the carbon fibre arm is not an easy task. In fact the mechanical structure of the link is complex and it was not possible to disassemble it to study each single part independently. However, since the inertia of the arm plays a key role in the feedforward torque, it needed to be estimated somehow. The adopted solution is based on the A-RISE controller. The regression matrix is now focused on the inertia of the arm and no more on the transported mass. In this way it is possible to estimate the inertia of the structure composed by motor, arm and elbow without the necessity of knowing the inertia of the single parts. The equation of the feedforward torque 3.9 has the same structure of equation 3.7 with the difference that now it is the inertia term to be estimated and not the mass of the mobile platform.

$$\tau_{FF}(t) = \ddot{q}_d(t)I_e - \cos(\alpha) \left(\frac{L_{arm}}{2} m_{arm} + L_{arm} m_e \right) + \left(J^T G + J^T \ddot{X} \right) m_p \quad (3.9)$$

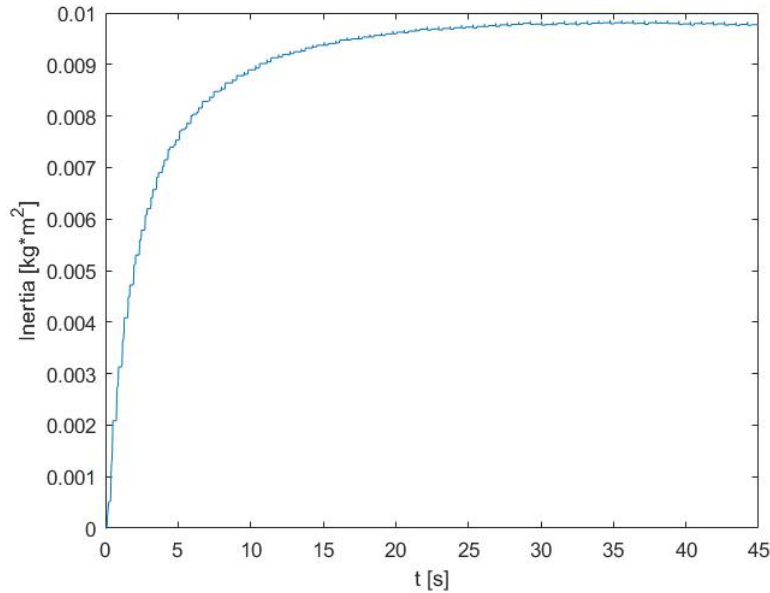
where I_e is the estimated inertia and it is defined as

$$I_e(t) = I_e(t-1) + \Gamma \dot{I}_e(t) \quad (3.10)$$

with $\dot{I}_e(t) = Y_d^T(\cdot)r(t)$.

The robot is assembled with carbon fibre arms, BAC forearms and the mobile platform without any transported mass. The RISE parameters are the same used in the previous situation, with the exception of $\Gamma = 0.0003$. The trajectory applied is simpler than the one of the previous experiment: semi-elliptic endless loop, back and forth from two different points. The acceleration applied is 2.5 G. The estimation of the inertia is shown in figure 3.8. The time required to reach steady-state condition is very long, approximately 30 s, and the average value at steady state is $I_e = 9.8 \cdot 10^{-3} \text{ kg} \cdot \text{m}^2$.

Figure 3.8. Carbon fibre arm inertia estimation



In order to prove the correctness of the estimation, another test has been performed in a different configuration. In this case a mass of 200 g has been attached at the end of each arm. Then the inertia has been estimated again with the same controller used in the previous situation. The purpose of the test is to check if the new value of the estimated inertia is coherent with the introduction of the mass. A simple schematic of the arm structure used in each test is shown in figures 3.9 and 3.10. The inertia estimation when the masses are attached to the arm is reported in figure 3.11.

Figure 3.9. Arm schematic

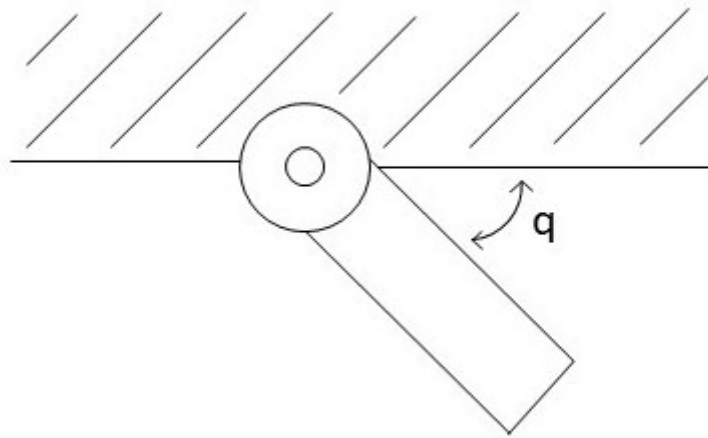


Figure 3.10. Arm and mass schematic

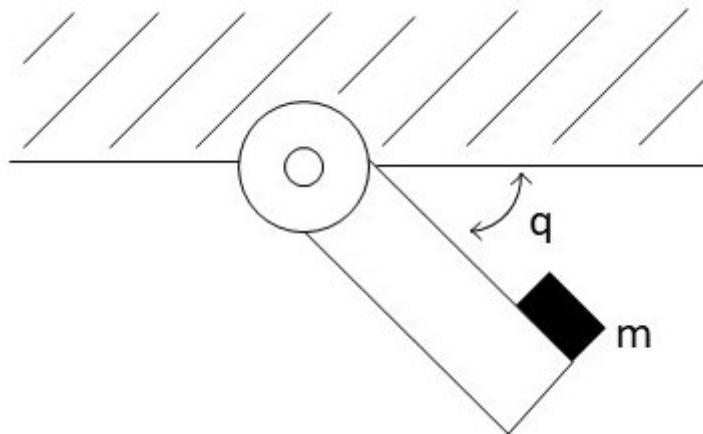
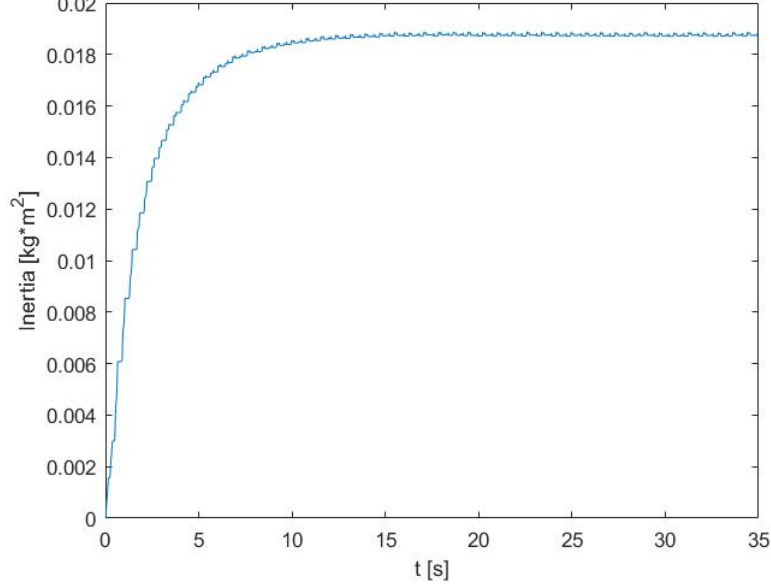


Figure 3.11. Carbon fibre arm and external mass inertia estimation



The final value of the inertia is $I_e = 18.7 \cdot 10^{-3} \text{ kg} \cdot \text{m}^2$. It can be observed that the final value is reached faster than in the previous case. This fact is due to the intrinsic structure of the adaptation term, which is based on the regression matrix and the combined error. As a consequence the higher the tracking error, the faster the estimation.

In order to compare the obtained result with the previous one, some assumptions have been made. The mass is considered as a point mass instead of a steel cylinder with $r = 1.5 \text{ cm}$ and $h = 3.6 \text{ cm}$. The distance between the centre of rotation and the point mass is $L = d_1 + \frac{h}{2} = 21.5 \text{ cm}$, where d_1 is the distance between the top base of the cylinder and the centre of rotation of the arm and h is the height of the cylinder. The variation of the inertia corresponds to the inertia of the mass I_m .

$$I_m = I_e - I_{arm} = 9.7 \cdot 10^{-3} \text{ kg} \cdot \text{m}^2 \quad (3.11)$$

where I_{arm} is the estimated value of the inertia of the arm found with the previous experiment. Since the inertia of a point mass rotating around a fixed point at distance L is given by $I = mL^2$, the mass can be computed inverting the formula, obtaining $m = 194.2 \text{ g}$. This result is very close to the real value of the mass applied and the difference can be traced back to the simplifying assumptions previously described. Thanks to this result, it has been proved that the controller is working as expected.

For sake of completeness, it is possible to estimate the inertia of the carbon fibre arm without considering the inertia of the motor and the elbow, that are already known.

$$I_{cb} = I_{arm} - I_{mot} - I_{elb} = 4.8 \cdot 10^{-3} \text{ kg} \cdot \text{m}^2 \quad (3.12)$$

where I_{elb} is obtained considering the 70% of the mass of the forearms as a point mass placed at the very end of the arm with respect to the centre of rotation. In this way the

inertia of the coupling placed on the end of the arm is included into the inertia of the carbon fibre arm. Motor inertia I_{mot} is taken from the data-sheet.

In conclusion, the estimation of the inertia is slow and it requires a lot of time. Because of that, the purpose of this controller is not to estimate every time on-line the inertia of the arm, but to estimate it once and for all and then integrate its value in the dynamic model used to compute the feedforward torque, with all the other parameters known a-priori.

Chapter 4

Comparison of different controllers in pick and place operations

In this experiment all the controllers previously examined are tested in case of a simple pick and place operation. The trajectory is very simple, the mass is moved in an endless loop between the extremities of a semi-elliptic trajectory represented in figure 4.1, since it is the best possible trajectory as reported in [8]. Figure 4.2 shows the Cartesian variables of the trajectory in case of an acceleration of 2.5 G. In order to have comparable results with the work of M. Bennehar [2] the sampling frequency is changed to 1 kHz and no filters have been applied. The reduction of the sampling frequency itself acts as a filter, in fact it is just above the Shannon's limit of the frequencies to be removed. Only the BAC forearms have been used in this experiment. The variation of the sampling frequency requires the controllers to be tuned again. The new parameters are reported in table 4.1. The controllers have been tested in three different situations. The first one consists in moving the mobile platform following the trajectory not transporting any mass, the second one with the load always attached and the third one picking and placing the mass. For each situation, different accelerations have been considered.

Table 4.1. Control parameters - Sampling frequency 1 kHz

ARM	PID			RISE and A-RISE				
	K_p	K_d	K_I	α_1	α_2	K_s	β	Γ
Aluminium	10	0.04	120	300	1.40	1.3	1.5	0.1
Carbon fibre	18	0.08	200	300	1.66	3.0	2.0	0.1

Figure 4.1. 3D trajectory

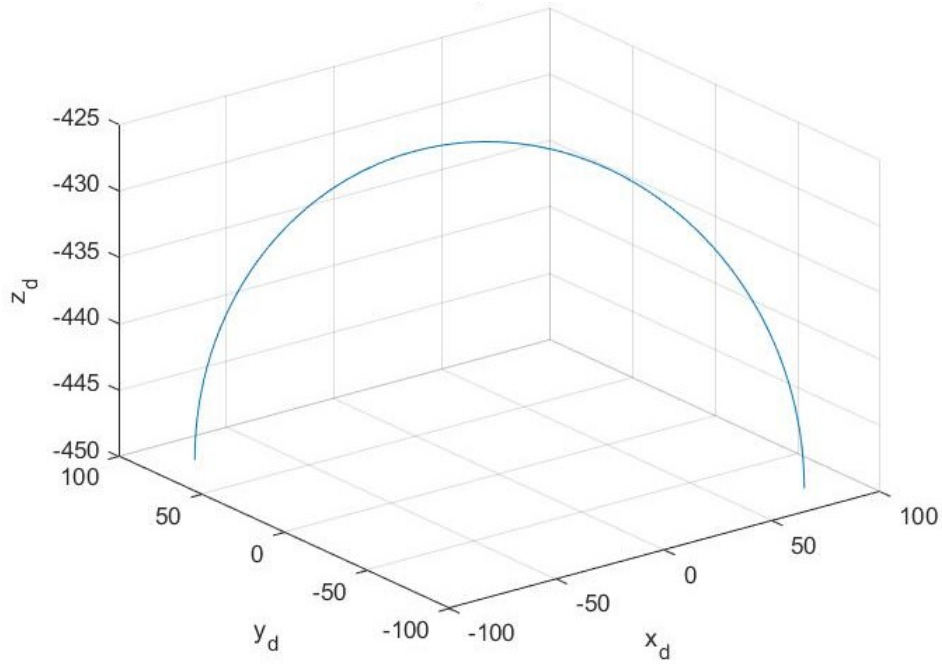
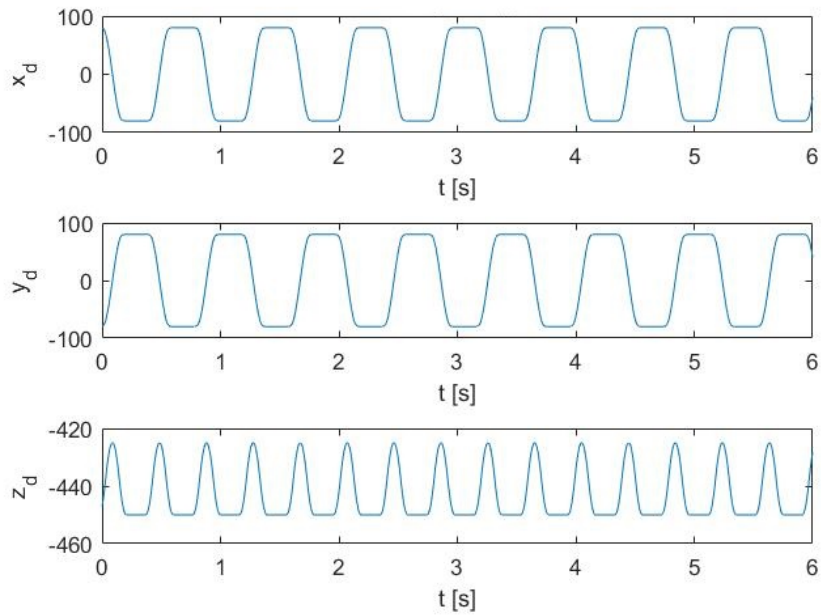


Figure 4.2. Cartesian variables - 2.5 G acceleration



4.1 Situation 1 - no mass transported

The first situation does not involve any transported mass. The mobile platform moves freely in the workspace. In the graphs 4.3 and 4.4, is reported the trend of the Cartesian RMSE with respect to the acceleration, which varies from 1 G up to 10 G. In figures 4.5, 4.6 and 4.7 are reported the peak errors in relation to the acceleration in case of carbon fibre arm. It can be observed that, in both cases, the RISE and the A-RISE controllers have approximately the same results. This is due to the fact that the mobile platform is not transporting any unknown mass and so all the dynamics are already included in the model made off-line. In this situation the controllers behave in different ways depending on the arm. In fact when the aluminium arm is present the RISE and A-RISE have better performances with respect to the PID. Instead using carbon fibre arms, thanks to the possibility of having higher gains, the PID guarantee results on the same level of the other two controllers.

Figure 4.3. Aluminium arm Cartesian RMSE

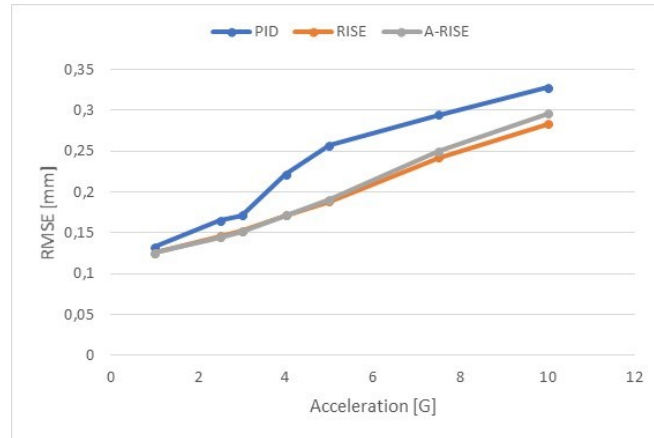


Figure 4.4. Carbon fibre arm Cartesian RMSE

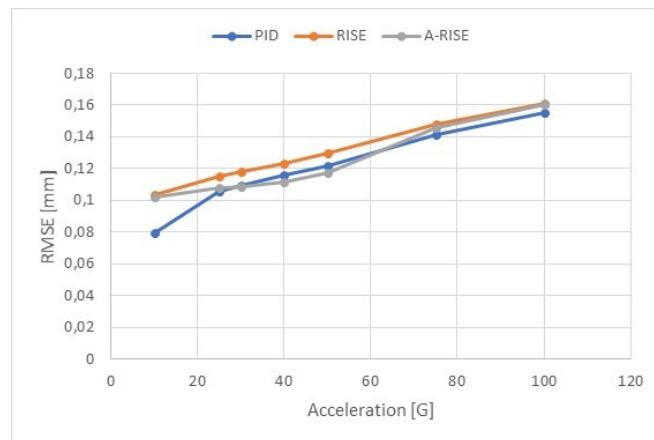


Figure 4.5. Carbon fibre arm, PID controller, peak errors

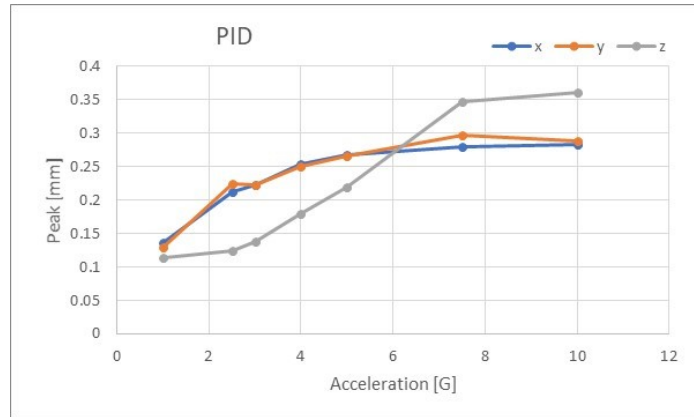


Figure 4.6. Carbon fibre arm, RISE controller, peak errors

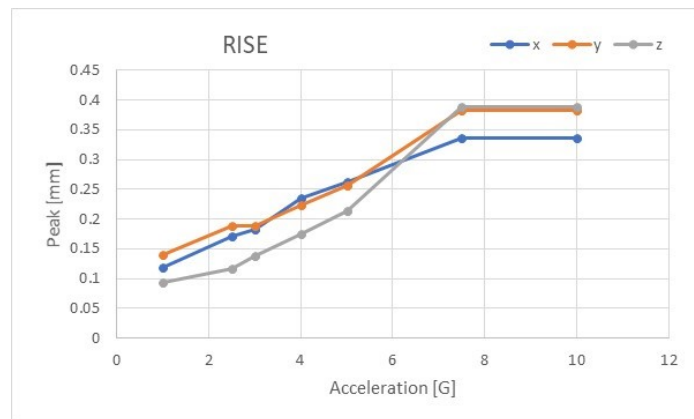
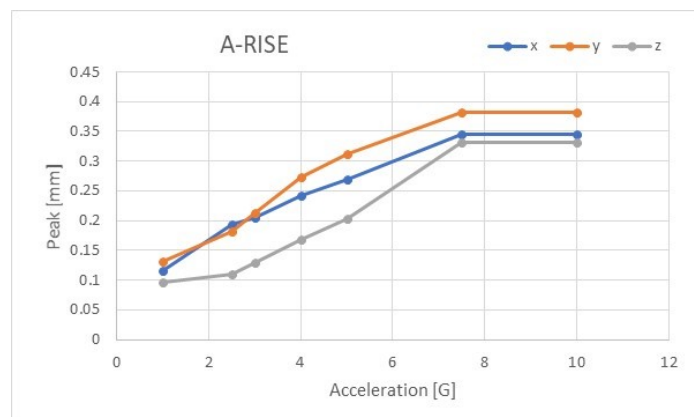


Figure 4.7. Carbon fibre arm, A-RISE controller, peak errors



4.2 Situation 2 - 225 g mass attached to the mobile platform

In this situation the mass has been attached to the mobile platform through a magnet, but it is not compensated by the feedforward torque. The trajectory applied is the same of the previous situation as well as the range of accelerations tested. Also in this case the RMSE in case of aluminium arms and then carbon fibre arms with respect to the applied acceleration are reported (Figures 4.8 and 4.9). In figures 4.10, 4.11 and 4.12 are reported the peak errors in relation to the acceleration in case of carbon fibre arm. The error increases, as expected, proportionally to the acceleration applied. The three controllers, in this situation, give different results. As expected, the better performances are obtained when the A-RISE is applied. In fact once it has estimated the transported mass, it is able to apply the right feedforward torque, minimizing the errors. It can also be observed that the RISE controller is able to compensate the unknown mass better than the PID, even without estimating its value, proving the great robustness of the RISE controller.

Figure 4.8. Aluminium arm Cartesian RMSE

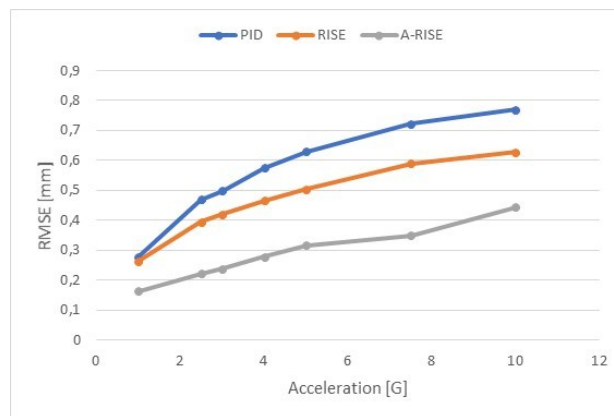


Figure 4.9. Carbon fibre arm Cartesian RMSE

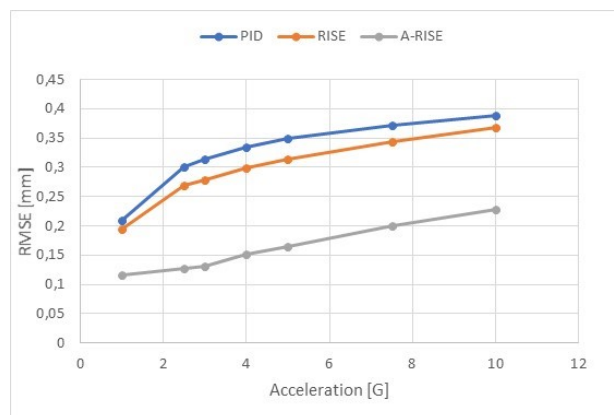


Figure 4.10. Carbon fibre arm, PID controller, peak errors

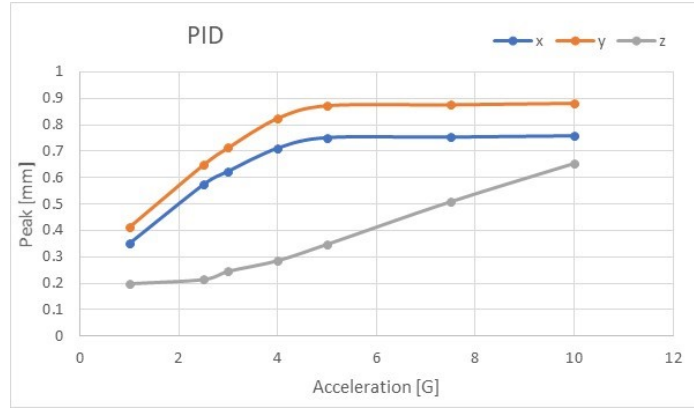


Figure 4.11. Carbon fibre arm, RISE controller, peak errors

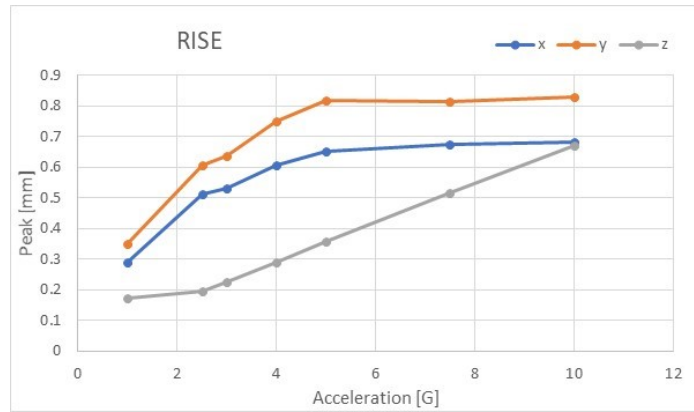
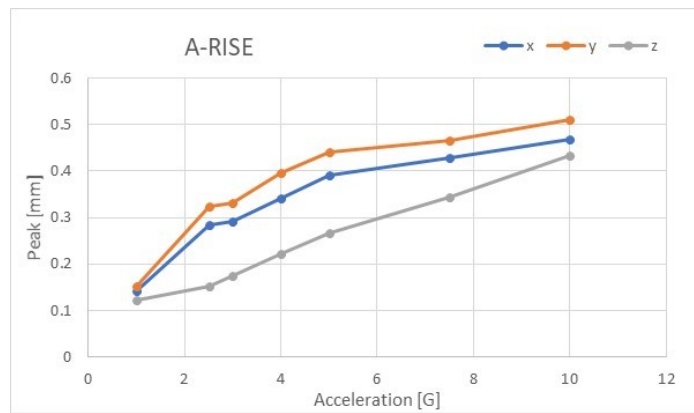


Figure 4.12. Carbon fibre arm, A-RISE controller, peak errors



4.3 Situation 3 - pick and place of a mass of 225 g

The trajectory applied is the same of the two previous situations, but now the mass is picked and placed in an endless loop, in fact it is moved back and forth between the positions of pick and place. It is not possible to know a-priori the value of the transported mass, because it changes through the time. As in the previous situations, it is plotted the RMSE with respect to the acceleration for both the arms, as shown in figures 4.13 and 4.14. In figures 4.15, 4.16 and 4.17 are reported the peak errors in relation to the acceleration in case of carbon fibre arm. Observing the graphs it can be noticed that the performances of PID and RISE controllers are almost the same. An improvement in the RMSE is present when the A-RISE controller is used. However the difference between the performances of the different controllers is less evident than in Situation 2. This is due to the fact that the A-RISE controller is not able to estimate correctly the transported mass regardless of the acceleration applied. In fact in order to estimate the mass, the A-RISE uses the regression matrix and the combined error. Low acceleration means low errors and as a consequence a slower estimation of the mass, which is not able to reach the actual value before the place operation. High acceleration, instead, causes bigger errors (so a faster estimation) but it reduces the time between pick and place operations. In any operative condition it is impossible to estimate correctly the mass because the time when the mobile platform is holding the load is too short. Moreover, increasing the acceleration causes to have the highest peak errors with the A-RISE controller. This unpredicted event is due to the poor estimation of the mass of the payload.

Figure 4.13. Aluminium arm Cartesian RMSE

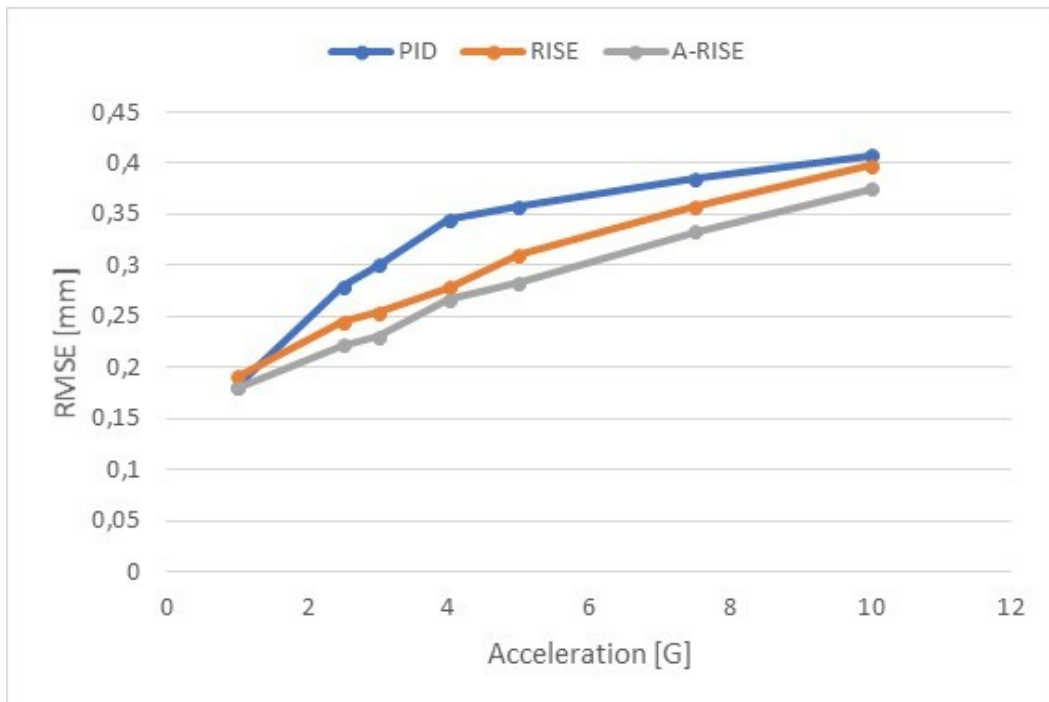


Figure 4.14. Carbon fibre arm Cartesian RMSE

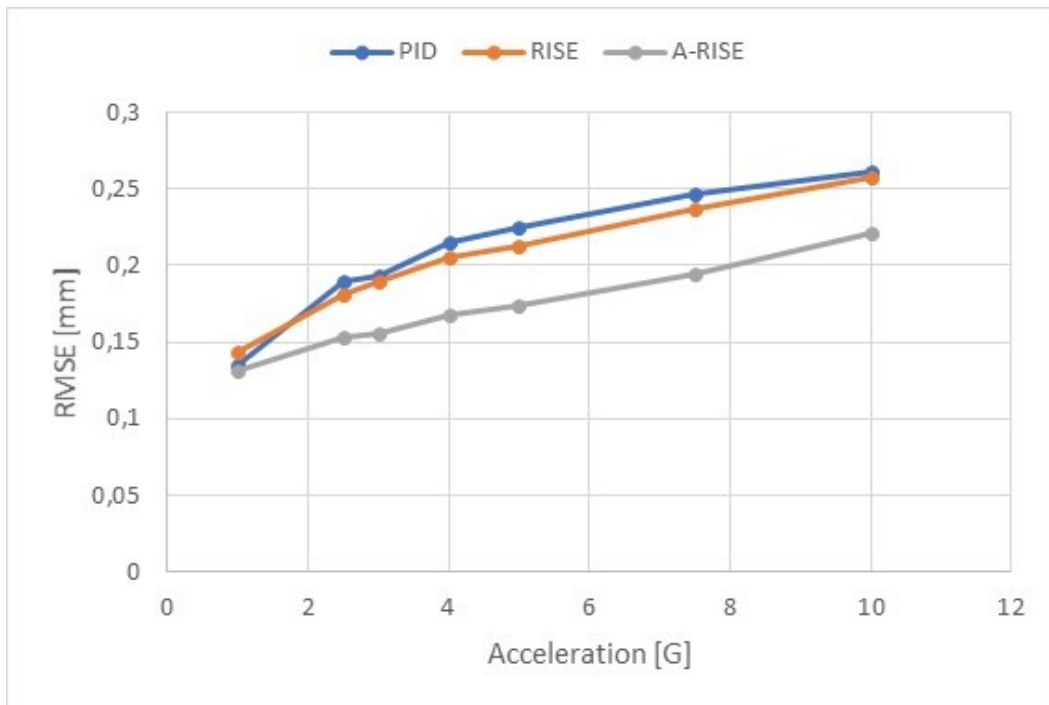


Figure 4.15. Carbon fibre arm, PID controller, peak errors

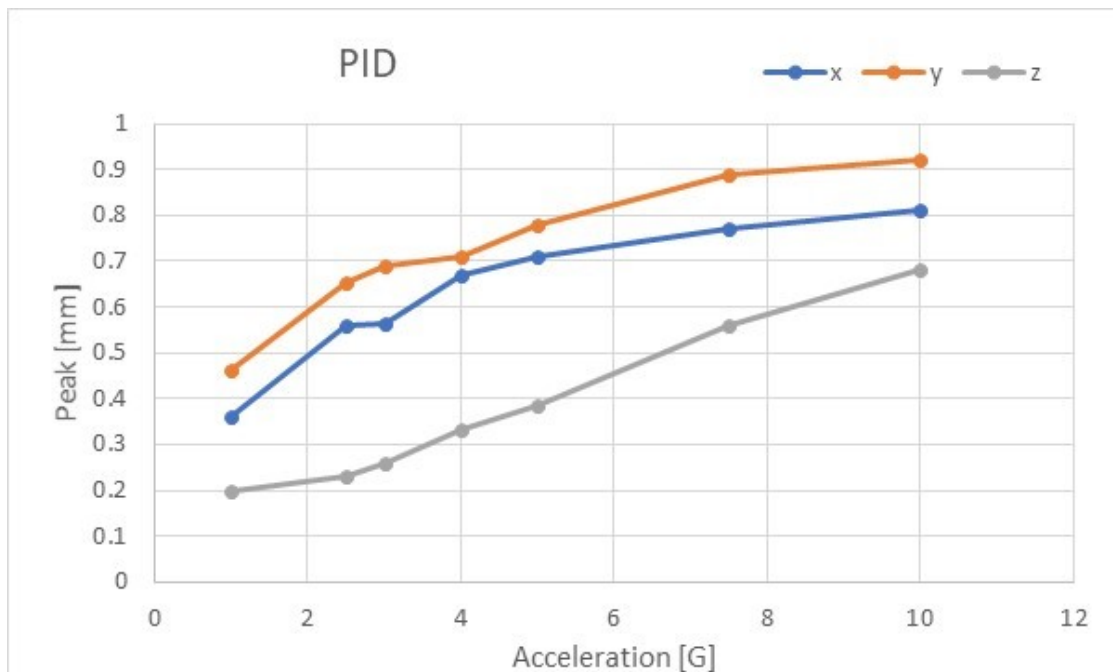
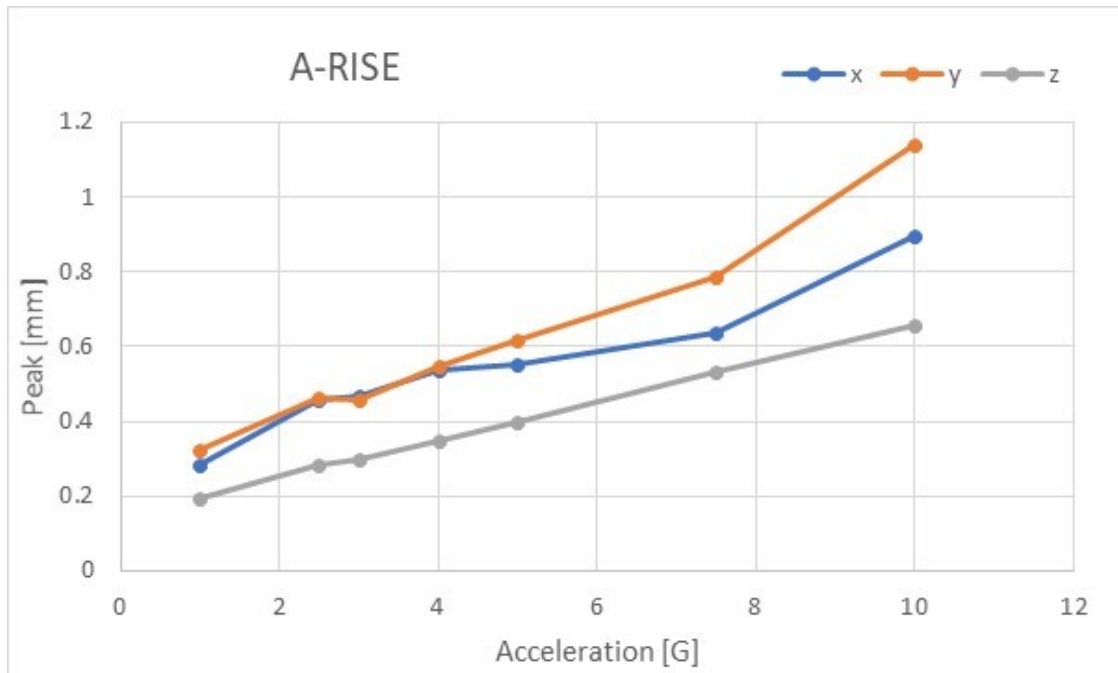


Figure 4.16. Carbon fibre arm, RISE controller, peak errors



Figure 4.17. Carbon fibre arm, A-RISE controller, peak errors



As it can be noticed in the picture 4.18, the trend of the estimation of the mass in time is not the expected one. In fact not only it never reaches the actual value of the transported mass, but when the mobile platform is moving without any mass attached (time interval between a place and the next pick), it does not return to zero. The system behaves in the same way as if a payload of around 140 g is always transported by the mobile platform. The adaptation mechanism increases the estimated value of the mass when it is transported and it tries to return to zero after the place operation, but without any success because the time required for this operation is too long with respect to the one available. In picture 4.19 is reported the evolution of the estimated mass with respect to the real value of the transported mass, during a single iteration. Two main considerations can be done observing this graph. First of all there is a delay between the transitions of the estimated value with respect to the real one. This is due to the fact that the estimation begins only when the mobile platform starts moving and so the time between the actual pick and the first movement is useless for the purpose of the mass estimation. Same consideration can be made for the place operation. In fact, in static conditions, the error is null thanks to the integral term of the RISE controller. The second observation is that the process of reduction of the estimated mass is even slower than the increasing one and it never goes even close to the zero. As a consequence the amplitude of the variation of the estimated mass is around 40 grams with respect of the 225 grams of the real case and the value oscillates around 140g.

Figure 4.18. Transported mass estimation

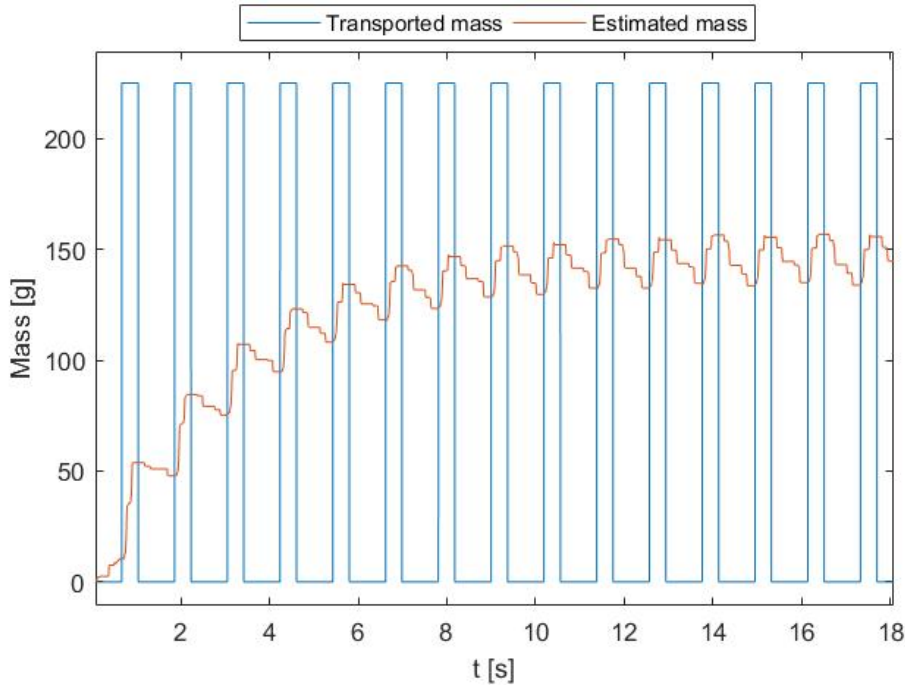
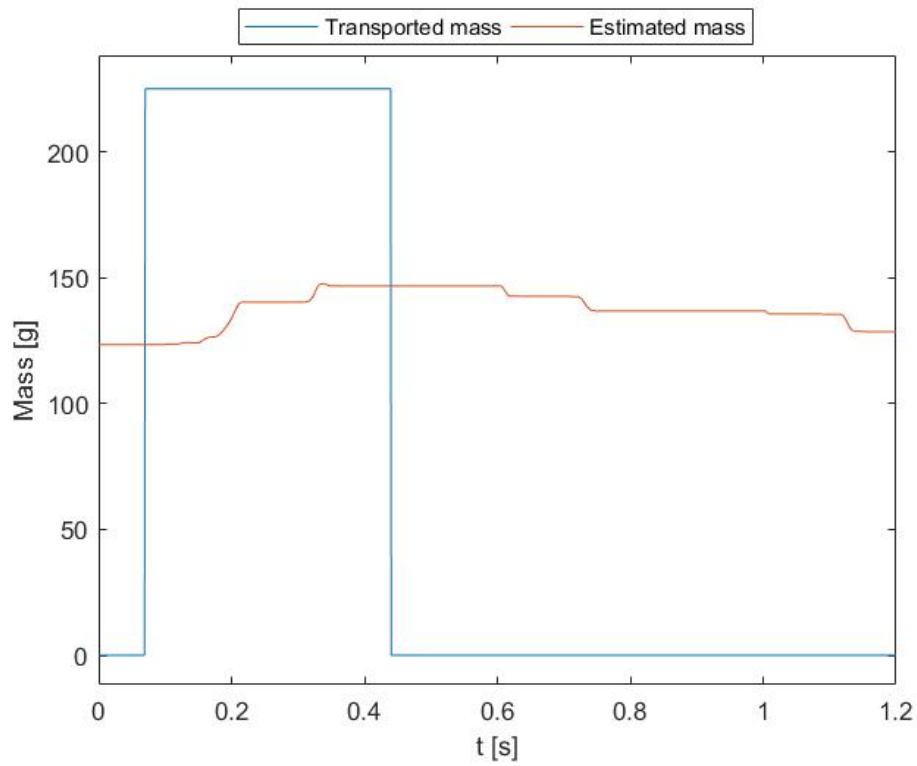


Figure 4.19. Transported mass estimation over a single iteration



In conclusion, although the best performances in terms of RMSE are obtained using the A-RISE controller, the improvement is below expectations and the trend of the estimated mass is not the expected one. Same results, in terms of RMSE, can be obtained with a normal RISE with a feedforward torque that considers a 140 g mass always attached to the mobile platform, because of that other solutions have to be investigated.

Chapter 5

Iterative learning controller

In pick and place operations, the trajectory applied is always the same, it is repeated endlessly and generally the value of the transported mass does not change through the iterations. Since the A-RISE did not give the desired results in terms of mass estimation, a new approach has been used, based on an iterative learning controller, ILC [6]. The controller is based on a PID structure and an external torque whose value is tuned iteration after iteration, depending on the value of the previous ones (Figure 5.1). The torque applied to the motor is given by the following equation:

$$\tau(t) = K_p e(t) + K_d \dot{e}(t) + K_I \int_0^t e(t') dt' + u(t) \quad (5.1)$$

$$u(t) = u(t-1) + \Lambda e(t) + \Gamma \dot{e}(t) \quad (5.2)$$

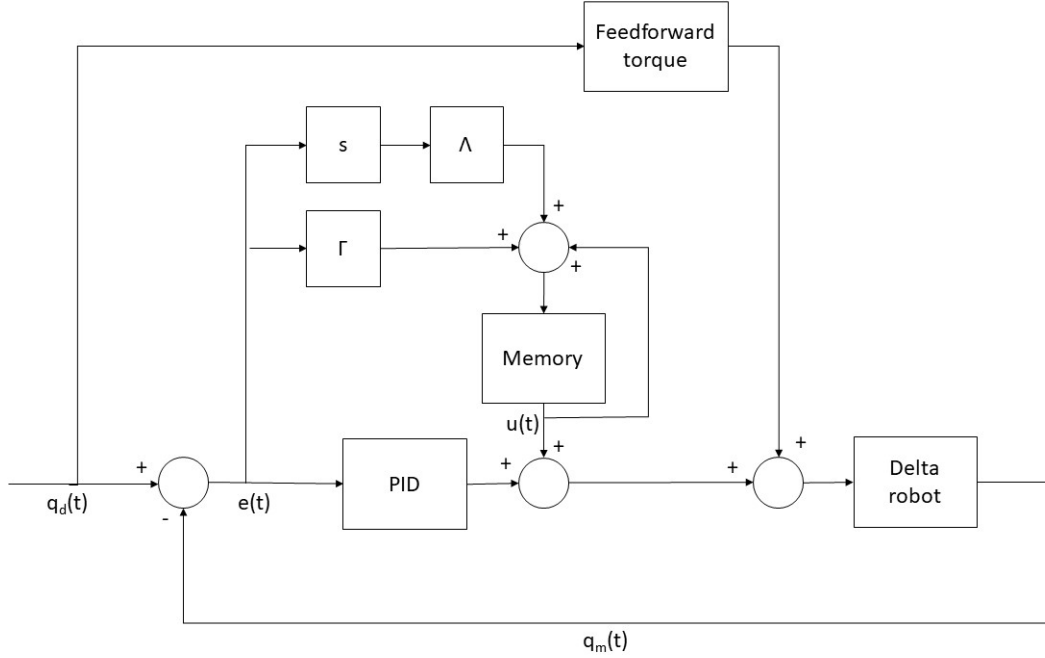
where $e(t) = q_d(t) - q_m(t)$, $\dot{e}(t) = \dot{q}_d(t) - \dot{q}_m(t)$, Λ and Γ are the two gains of the memory element. The tuning of those two parameters has been found by trial and error, with the knowledge that higher values bring to a faster convergence but also an increase of the oscillations at low frequency. The robot is assembled with BAC forearms and the mobile platform with a magnet attached to it. The arms change according to the performed test. The sampling frequency is 1 kHz and the HAL timer is 100 μs . The values of the used parameters used reported in table 5.1.

Table 5.1. ILC parameters - sampling frequency 1 kHz

Arms	K_p	K_d	K_I	Λ	Γ
Aluminium	10	0.04	120	0.10	0.01
Carbon fibre	18	0.08	200	0.10	0.01

The controller has been tested in three different situations. In the first case the transported mass is absent, in the second one it is always attached to the mobile platform, while the third one is a real pick and place operation. The trajectory applied is the same of the previous chapter. Only the case with 10 G acceleration has been tested for the first two situations and 2.5 G for the last one.

Figure 5.1. ILC control loop



5.1 Situation 1 - no mass transported

The first situation where the controller has been tested is the classical trajectory of the previous chapter, without any transported mass. The robot has been configured with aluminium arms and BAC forearms, because it was the case where the PID was giving the worst results with respect to the other two controllers. The obtained results are reported in figures 5.2 and 5.3. Although the number of iterations required to is quite high, eventually the controller is able to reduce the error considerably (Table 5.2). Now with the ILC it is possible to have the smaller RMSE of among all the tested controllers (Figure 4.3). The drawback is an evident increment of high frequency oscillations that can be noticed in figure 5.3 between 0.4 and 0.6 s.

Table 5.2. RMSE [mm] - 10 G acceleration - Trajectory of Figure 4.1

Iteration n.1	Iteration n. 900	Improvement %
0.3228	0.1661	48.54

Figure 5.2. RMSE trend - 10 G acceleration - Trajectory of Figure 4.1

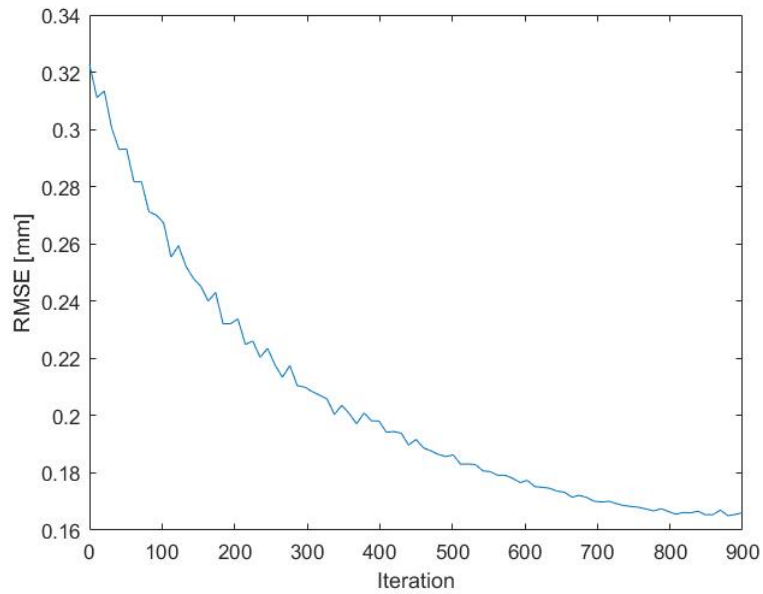
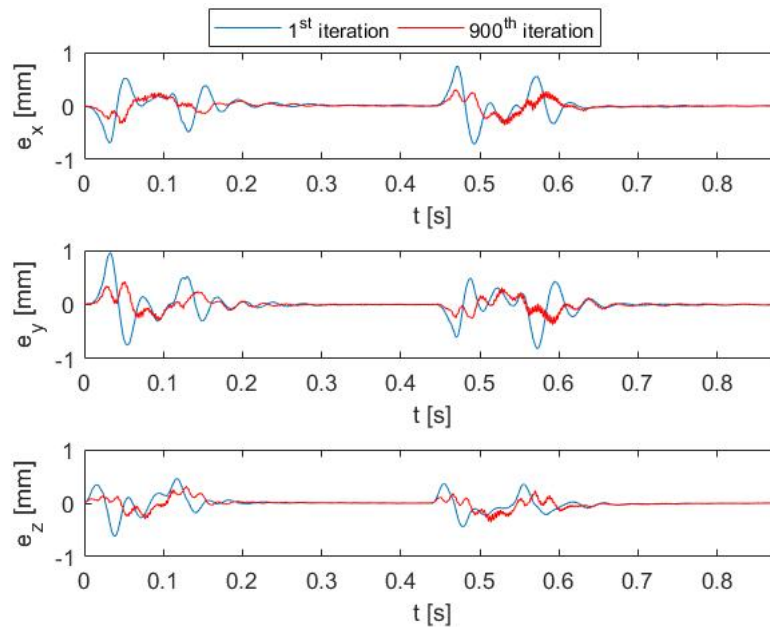


Figure 5.3. Tracking error - 10 G acceleration - Trajectory of Figure 4.1



5.2 Situation 2 - 225 g mass attached to the mobile platform

Because of the interesting results obtained in the previous section using aluminium arms, now the robot has been assembled with the carbon fibre ones in order to verify if it is possible to obtain the same results. Since it has been observed that the ILC is less effective when the RMSE is already small, in this situation a mass of 225 g has been attached to the mobile platform. The inverse dynamic model is not aware of the presence of this mass. The results are reported in figures 5.4 and 5.5. The first graph displays the RMSE with respect to the number of iterations. It can be easily noticed that the number of iterations required to reduce the RMSE of 30% is extremely high, around 2600. The RMSE converges to a value and it do not decrease any more (Table 5.3). This is also made more evident by the fact that the resonance frequency of the robot starts being excited. In fact high frequency oscillations can be observed in the x and z axes of the error of the 2600th iteration (Figure 5.5).

Table 5.3. RMSE [mm] - 10 G acceleration - Trajectory of Figure 4.1

Iteration n.1	Iteration n. 2600	Improvement %
0.3611	0.2438	32.48

The great number of iterations required to reduce the RMSE and the high precision necessary to define the iteration period, make the usage of this controller very difficult in case of real pick and place operations. Nevertheless a real pick and place test has been performed but, as expected, the results were not satisfactory at all.

Figure 5.4. RMSE trend - 10 G acceleration - Trajectory of Figure 4.1

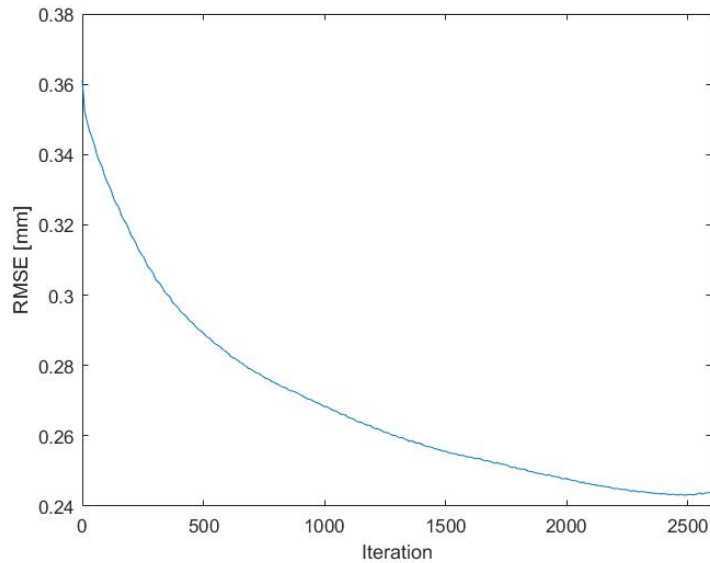
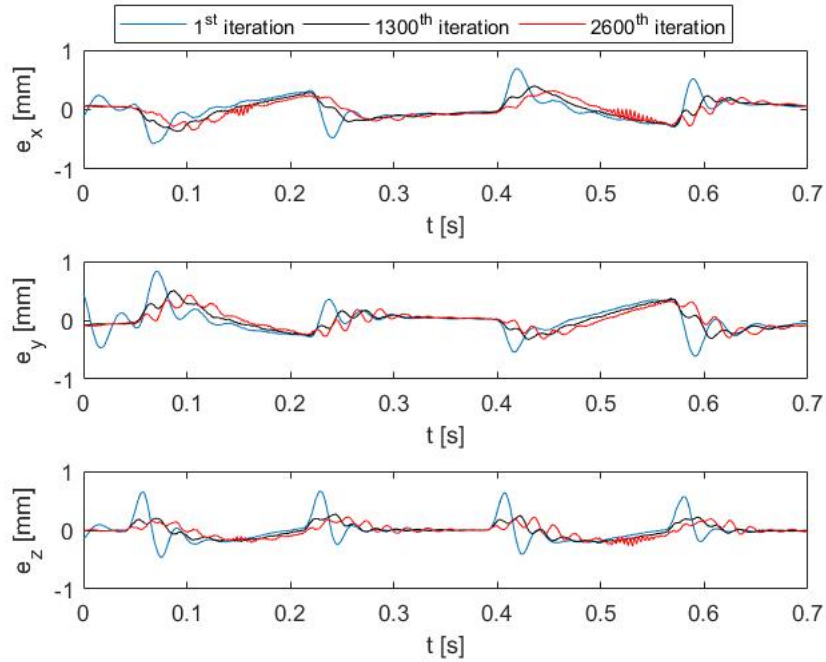


Figure 5.5. Tracking error - 10 G acceleration - Trajectory of Figure 4.1



5.3 Situation 3 - pick and place of a mass of 225 g

In this case the mass of 225 g is moved back and forth between the pick and place positions, in an endless loop by means of a semi-elliptic trajectory. An acceleration of 2.5 G has been chosen for this experiment. As expected the results were not satisfactory. In fact the reduction of the RMSE, with respect to the number of iterations, is even slower than in the previous case and to make matters worse another complication appeared: the period of each iteration is not constant any more. This is due to the fact that the time required to activate and deactivate the magnet varies through time. This fact can be observed in both graphs (figures 5.6 and 5.7). The oscillations of the iteration period are of the order of 2 ms. After 250 iterations, where the oscillations of the period compensate themselves, a series of shorter iterations appears. This reduction, that cannot be observed by the human operator, is sufficient to shift the waveform with respect of the previous ones. As a consequence not only the effect of the memory of the controller becomes useless, but it even worsens the performances. In fact since the error peaks are completely misaligned, the feedforward torque deriving from the memory element is misaligned too, opposing rather than helping the feedforward torque derived by the dynamic model. The shift can be clearly observed from the picture 5.7, while picture 5.6 shows the increase of the RMSE after the misalignment of the iterations.

In conclusion, the slowness of the reduction of the RMSE and the impossibility to have iterations with constant period, make this controller useless for the purposes of pick and place operations. Moreover the repeatability of the results is not granted. In fact the

misalignment of the signals appears after a different amount of iterations every time the test is performed.

Figure 5.6. RMSE trend - 2.5 G acceleration - Trajectory of Figure 4.1

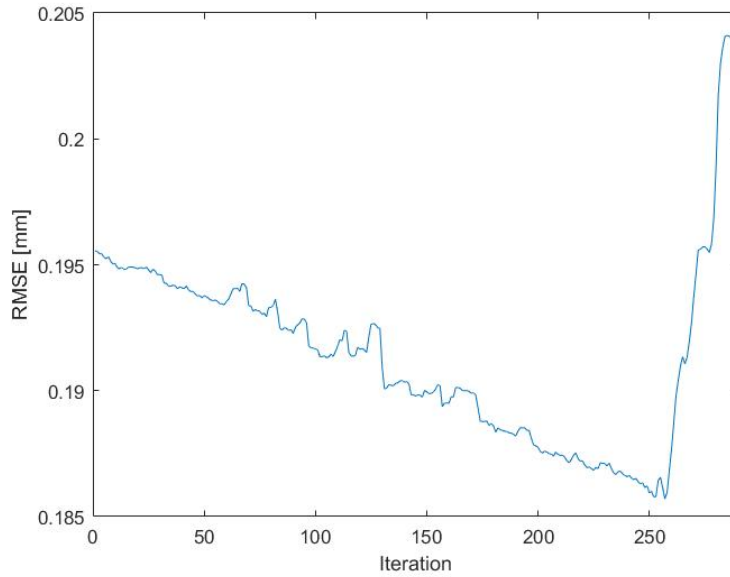
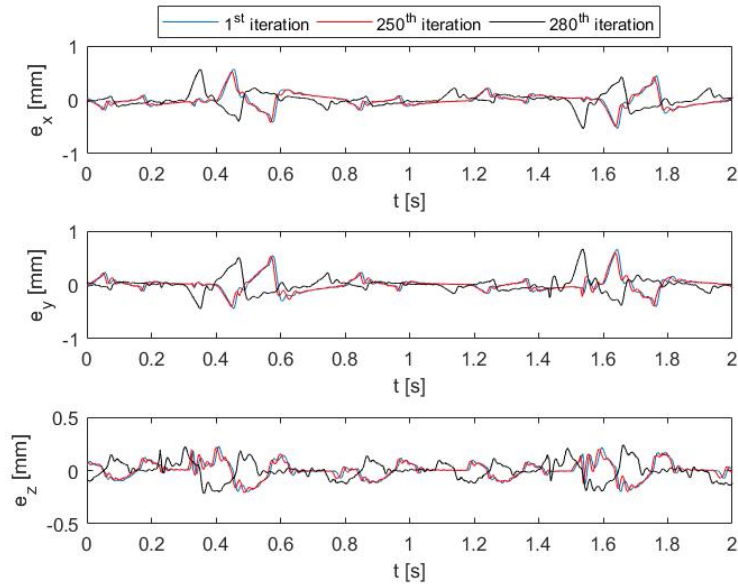


Figure 5.7. Tracking error - 2.5 G acceleration - Trajectory of Figure 4.1



Chapter 6

Conclusion

The principal objective of this work was to investigate which control system could guarantee the best performances in fast pick and place operations as carried out by a direct drive Delta robot.

The two aspects analysed in depth were

- Advanced control systems (PID, RISE, A-RISE, ILC)
- Material of specific physical components

Results were to a degree unexpected and significantly interesting. First of all I could verify that the adopted controllers, which appeared to work properly in both simulations and publications, proved unable to meet expectations under real circumstances and accurate testing. All weak points of each controller are summarised with the intent of providing a solid and certain basis for further research. The principal outcome can be described as follows.

1) The proportional-integral-derivative (PID) and the robust integral of signum of error (RISE) controller do not pose a specific problem; as a matter of fact their inefficiency is only due to the absence of an adaptive term able to compensate the variation of the transported mass through the iteration. 2) The issue with the adaptive RISE (A-RISE) is the estimation time needed with respect to the time span available during the payload transportation phase. Moreover, the time required to recognise the no-load condition - e. g. the time interval between the placing operation and the picking one - is even longer. 3) Lastly, the iterative learning controller (ILC) proved to be able to reduce the error (especially in the case of the Cartesian RMSE) exclusively under limit conditions and after a number of iterations too high for real applications.

Material-wise the project offered convincing and reliable results. The manipulator performances obtained by using carbon fibre arms were definitely better than those achieved by means of aluminium arms (Cartesian RMSE reduced by more than 50 %). Such outcome derives from the combination of higher control gains and the fact that the carbon fibre resonance frequency is kept under control - the latter being higher than the aluminium's. Add to that, the carbon fibre arm is more effective in terms of bending oscillations when the manipulator is in action with high accelerations, thus making the robot more controllable and increasing the dynamics of the robot operations.

During my testing exercises, I also happened to observe that the resonance frequency of the robot was varying according to the position of the mobile platform in the workspace. Therefore I suggest that it might be useful to investigate the relationship between physical position and frequency of resonance with the aim of obtaining an adaptive notch filter, in which the frequency cut should be a function of the position of the end effector in the space. Thus the dynamic of the system would not be limited by a wide bandstop filter, probably allowing better performances.

Bibliography

- [1] L. Villani G. Oriolo B. Siciliano, L. Sciavicco. *Robotics - Modelling, Planning and Control*. Springer, 2009.
- [2] M. Bennehar, A. Chemori, M. Bouri, L. F. Jenni, and F. Pierrot. A new RISE-based adaptive control of PKMs: design, stability analysis and experiments. 91(3):593–607.
- [3] M. Bennehar, A. Chemori, and F. Pierrot. A novel rise-based adaptive feedforward controller for redundantly actuated parallel manipulators. In *2014 IEEE/RSJ International Conference on Intelligent Robots and Systems*, pages 2389–2394, Sept 2014.
- [4] B. Bidikli, E. Tatlicioglu, and E. Zergeroglu. A self tuning rise controller formulation. In *2014 American Control Conference*, pages 5608–5613, June 2014.
- [5] B. Bona. *Dynamic Modelling of Mechatronic Systems*. Celid, 2013.
- [6] C. E. Boudjedir, D. Boukhetala, and M. Bouri. Fuzzy logic iterative learning control for trajectory tracking of parallel kinematic manipulators. In *2017 5th International Conference on Electrical Engineering - Boumerdes (ICEE-B)*, pages 1–6.
- [7] R. Clavel. Device for the movement and positioning of an element in space, 1990.
- [8] Alain Codourey. Dynamic modeling of parallel robots for computed-torque control implementation. *The International Journal of Robotics Research*, 17(12):1325–1336, 1998.
- [9] John J. Craig, Ping Hsu, and S. Shankar Sastry. Adaptive control of mechanical manipulators. *The International Journal of Robotics Research*, 6(2):16–28, 1987.
- [10] A. Bashir E. Castillo Castenada, G. Garcia. Delta robot: Inverse, direct, and intermediate jacobians. 220:103–109, 01 2006.
- [11] G. Ellis. *Control System Design Guide*. Elsevier, 2004.
- [12] K. Youcef-Toumi H. Asada. *Direct-Drive Robots - Theory and Practice*. The MIT Press, 1987.
- [13] P. M. Patre, W. MacKunis, C. Makkar, and W. E. Dixon. Asymptotic tracking for systems with structured and unstructured uncertainties. In *Proceedings of the 45th IEEE Conference on Decision and Control*, pages 441–446, Dec 2006.
- [14] M. Rachedi, M. Bouri, and B. Hemici. Feedback control for parallel mechanism and application to delta robot. In *22nd Mediterranean Conference on Control and Automation*, pages 1476–1481, June 2014.
- [15] D. Schlichtarle. *Digital Filters - Basics and Design*. Springer, 2011.
- [16] B. Xian, D. M. Dawson, M. S. de Queiroz, and J. Chen. A continuous asymptotic tracking control strategy for uncertain multi-input nonlinear systems. In *Proceedings of the 2003 IEEE International Symposium on Intelligent Control*, pages 52–57, Oct 2003.

- [17] K. Youcef-Toumi and H. Asada. Design and control of direct-drive arms. In *1985 American Control Conference*, pages 696–702, June 1985.